Final Report

NAG1-01004

Graphite Nanoreinforcements for Aerospace Nanocomposites

submitted to:

Dr. Jeffrey A. Hinkley
NASA Langley Research Center
Hampton, VA 23681-2199
(757) 864-4259, FAX -8312
Email: Jeffrey.A.Hinkley@nasa.gov

submitted by:

Lawrence T. Drzal

University Distinguished Professor
College of Engineering
Composite Materials and Structures Center
Michigan State University
517-353-5466

drzal@egr.msu.edu

October 25, 2005
Revised January 25, 2006

Table of Contents

Abstract 3
Project Description 4
Background 4
Objectives 5
Significance 5
Previous Work Done On Graphite Platelet Nanocomposites 6
Research Project Plan 8
Research Project Results 11
Exfoliation of Exfoliated Graphite 13
Pulverization of Exfoliated Graphite 15
Surface chemistry 16
Surface Treatments 21
O_2 Plasma Treatment 21
Nitric Acid Treatment 21
Ozone/Heat Treatment 21
UV/Ozone Treatment 22
TEPA Grafting Treatment 22
Acrylamide Grafting Treatment 22
Thermoset Composite Fabrication 24
Reinforcements for comparison 25
Composite Flexural Mechanical properties 27
Effect of size of exfoliated graphite platelets on flexural properties 27
Effect of surface treatments on flexural properties 28
Comparison with available carbon materials 30
Dynamic Mechanical Analysis 31
Thermomechanical analysis (TMA) 32
The effect of surface treatments on CTE 32
Electrical properties 34
Effect of graphite platelet size 34
Effect of surface treatment condition of graphite platelets 34
Comparison of various carbon materials 34
Microwave Exfoliated Nano Graphite Platelets 35
Thermal conductivity 37
Dielectric properties 38
Stress analysis in particulate composites 40
Description of Finite Element Models 42
Edge Angle Model 42
Filler Shape Model 43
Aspect Ratio Model 44
Distance Between Aligned Fillers 45
Finite Element Results 46
Effect of the Edge Angle on the Maximum Effective Stress 46
Effect of Filler Shape on Interface Stresses 48
Effect of Aspect Ratio on Interface Stress Condition 51
Effect of Distance between Aligned Fillers on the Interface Stress 53
Effect of Distance between Parallel Fillers on the Interface Stress 53
SUMMARY 58
REFERENCES 59

ABSTRACT

New advances in the reinforcement of polymer matrix composite materials are critical for advancement of the aerospace industry. Reinforcements are required to have good mechanical and thermal properties, large aspect ratio, excellent adhesion to the matrix, and cost effectiveness. To fulfill the requirements, nanocomposites in which the matrix is filled with nanoscopic reinforcing phases having dimensions typically in the range of 1nm to 100nm show considerably higher strength and modulus with far lower reinforcement content than their conventional counterparts. Graphite is a layered material whose layers have dimensions in the nanometer range and are held together by weak Van der Waals forces. Once these layers are exfoliated and dispersed in a polymer matrix as nano platelets, they have large aspect ratios. Graphite has an elastic modulus that is equal to the stiffest carbon fiber and 10-15 times that of other inorganic reinforcements, and it is also electrically and thermally conductive. If the appropriate surface treatment can be found for graphite, its exfoliation and dispersion in a polymer matrix will result in a composite with excellent mechanical properties, superior thermal stability, and very good electrical and thermal properties at very low reinforcement loadings.

The objectives of this research project were to modify the surface chemistry of exfoliated graphite nano-platelets (xGnP) in a thermoset matrix polymer and to investigate the factors that control the intercalation, exfoliation, dispersion and adhesion in polymer matrix composites. The approach taken consisted of two parts:

(1) Determination of the factors in a graphite platelet-epoxy system that control the adhesion at the atomic scale, molecular scale and macro scale.
(2) Improvement in the properties of the nanocomposites by designing an optimal surface chemistry.

Results obtained at concentrations of xGnP of less than 3 volume percent in an epoxy matrix have increased the flexural modulus (35%) and strength, reduced the coefficient of thermal expansion (50%), increased electrical conductivity (10exp+10), and increased thermal conductivity (10x).

Finite element analysis of the xGnP platelet has led to the following conclusions:

• Fillers with circular, ellipsoidal, or other rounded shapes should be better reinforcements in terms of minimizing the stress concentration.
• Fillers with higher aspect ratios introduced higher stress concentrations.
• High stress concentration was produced when nanofillers were aligned and located close to each other.
• The stress concentration was minimized when nanofillers were located parallel to each other at an optimal distance since stress could transfer from one filler to another.

To make the material conductive without sacrificing strength, it is necessary to arrange fillers close together, but in parallel positions so that they do not introduce a high stress concentration. The simulations revealed that there was an optimal distance for parallel-filler systems, which appeared to be around 2 to 4 times the thickness of the fillers. Thus the thickness of the fillers should be 5 nm or less.

An economic analysis of xGnP indicates that the xGnP nanoparticles could be produced at a cost in the ~$5 per pound range, making it cost effective compared to other nanoparticles such as carbon nanotubes.

PROJECT DESCRIPTION

Background. New advances in the reinforcement of polymer matrix composite materials are critical for advancement of the aerospace industry. Basically there are three factors to be considered: reinforcements, matrices, and adhesion between them. Good reinforcements are required to have good mechanical and thermal properties, large aspect ratios, and cost effectiveness. To fulfill these requirements, much attention has been paid in the last ten years to a new concept called nanocomposites. [1,2,3] A nanocomposite is a composite in which a matrix is filled with nanoscopic reinforcing phases having dimensions typically in the range of 1nm to 100nm. Polymer-ceramic composites made by sol-gel processes, [4,5,6,7,8,9] polymer-cellulose whisker composites [10,11,12], and polymer-clay composites [13,14] are examples of this category. These composites show considerably higher strength and modulus with far lower reinforcement content than conventional counterparts [15,16].

Polymer-clay composites also have some unique properties like high temperature resistance [17] and gas barrier properties [18,19]and are considered to be very useful in applications such as accessories for automobiles, structural components for portable electronics, and films for food packaging. Their unique properties are due mainly to the unique properties of platelet type reinforcements that have closely stacked layered structures comprised of silica and alumina sheets joined together. Once these layers are exfoliated and dispersed in a polymer matrix as platelets, they show excellent mechanical properties and preferable aspect ratios in addition to good thermal properties and cost effectiveness [20,21]Key points for fabricating good clay-polymer nanocomposites are intercalation of the polymer into clay galleries and exfoliation of the clay platelets in the matrix polymer. These phenomena are considered to be related to the adhesion between the reinforcement and matrix. Many fabrication methods have been proposed and some of them have achieved good results for clay-nylon 6 and clay-epoxy systems, but the basic factors that control these phenomena are unclear so that the maximum properties of the composite may not have been achieved.

Graphites are also layered materials whose layers are held together by weak Van der Waals forces. The same nanoreinforcement concept can be applied to create graphite platelet reinforced polymer composites. However graphite has an elastic modulus that is 10-15 times that of clay. Graphite is the stiffest material found in nature (Young's Modulus = 1060 MPa). Indeed, carbon (graphite) fibers are the stiffest macro reinforcing fiber available and are the backbone of the aerospace composite industry. Compared to nanoclays, nanographite platelets also have excellent electrical and thermal conductivity.

Graphite platelets have been known as host materials for intercalated compounds for many years. Some of the graphite-intercalated compounds (GICs) can be exfoliated by heating. These exfoliated graphite materials have been used as reinforcements for polymer composites, but primarily for increasing the electrical conductivity. Most of them have relatively poor mechanical properties because of poor separation of the exfoliated graphite sheets and the existence of many voids trapped in the composites. If the appropriate surface treatment can be found for graphite, its exfoliation and dispersion in a polymer matrix will result in a composite with mechanical properties far superior to any clay nanocomposite and in addition, superior electrical properties and thermal properties, opening up new applications such as electromagnetic shielding, high efficiency and isotropic thermal conductors, conductive polymers, etc.

Objectives. The objectives of this research project are to manipulate the surface chemistry of graphite platelets and investigate the factors that control their intercalation, exfoliation, dispersion and adhesion in polymer matrix composites. Once the relationships among these basic factors are established, composite mechanical properties will be optimized by controlling the platelet concentration, adhesion, and orientation.

Goals of this project are:

(1) Determine the factors that control the adhesion in the graphite platelet-epoxy system at the atomic, molecular, and macro scales.
(2) Establish the relationship between adhesion and mechanical and physical properties of the nanocomposites.
(3) Improve the properties of the nanocomposites by designing optimal surface chemistry.

Significance. Nanoreinforcements and nanocomposites offer the promise of creating new classes of composite materials for aerospace applications. Graphite platelet nanoreinforcements have the potential for providing substantial increases in the structural properties of aerospace polymers as well as the thermal and electrical properties. The relationships between the graphite surface chemistry, dispersability in polymer matrices, adhesion and composite mechanical properties discovered as a result of this program will identify new materials as well as new opportunities for their use. Furthermore, these structure-processing-properties relationships can serve as the foundation for computational models for nanocomposite materials.

PREVIOUS WORK ON GRAPHITE PLATELET NANOCOMPOSITES

Based on a thorough review of the literature, ours appears to be the only group investigating exfoliated graphite nanoreinforcements for polymers at the time the proposal was submitted.

Preliminary work by the author at Michigan State University explored the fabrication and mechanical properties of exfoliated graphite reinforced composites. Graphite flake samples were swelled with acid and exfoliated at high temperature so that the volume occupied by the graphite was increased dramatically. X-ray diffraction (XRD) plots shown in Figure 1 below were taken before and after treatment. Notice that the signal had dropped by a factor of 20 and the peak at 2.7 nm has almost disappeared. A new small peak at 2.2 nm is detected indicating

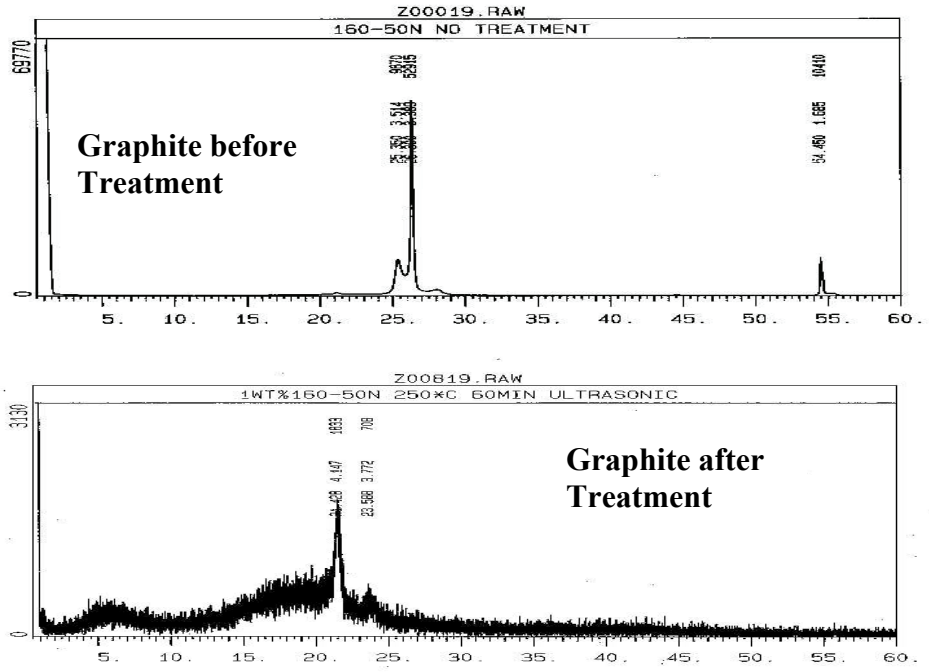

Figure 1. Xray Diffraction Data before and After Exfoliation of Graphite

that the graphite was intercalated and exfoliated after treatment.

The exfoliated graphite was ground into fine particles and added to an epoxy system at concentrations of less than 1 weight % as follows.
First, an aliquot of the exfoliated graphite was added into the epoxy system. [Epoxide: Shell Chemicals EPON^{TM} 828 (DGEBA), Curing Agent: Huntsman Cooperation JEFFAMINE^{TM} T403. The weight ratio of EPON^{TM} 828 to JEFFAMINE^{TM} T403 was 100 to 45. A reference sample of the same epoxy system without graphite was prepared from the same batch. The mixtures were cured by heating at 85ºC for 2 hours followed by 150ºC for 2 hours. The heating ramp rate was 3ºC per min. The microstructure of the composite was investigated by XRD, LSM, and TEM. Samples from five different batches were collected and investigated by both DMA and Tensile tests.

Figure 2 is the Laser Confocal Scanning Micrograph Image of the composite. Transmission mode images revealed that no light could be transmitted through the composite. This is because exfoliated graphite platelets are well dispersed in the matrix and they block the laser beam. Fluorescence mode reflection images show that most of the platelets are 20um or smaller while some of them are 50-100um.

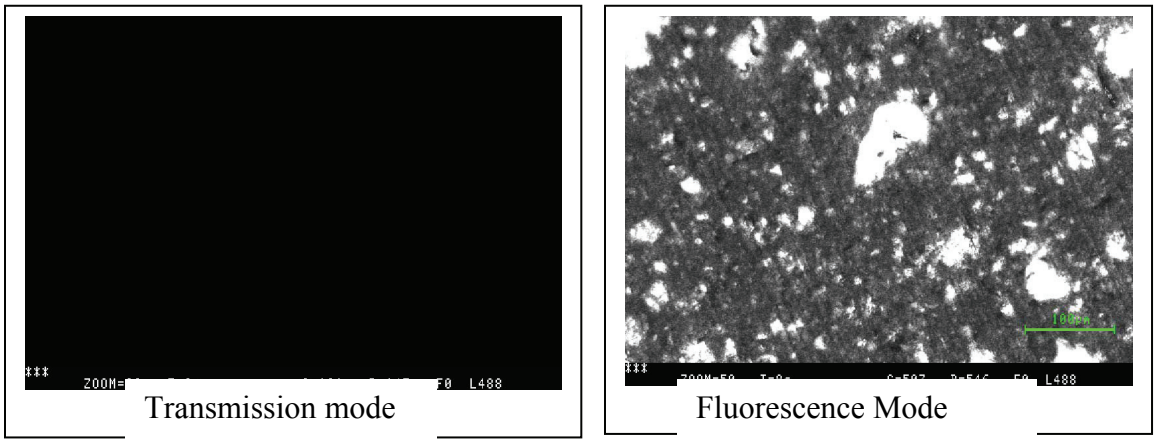

Figure 2. LSM image of the Composite

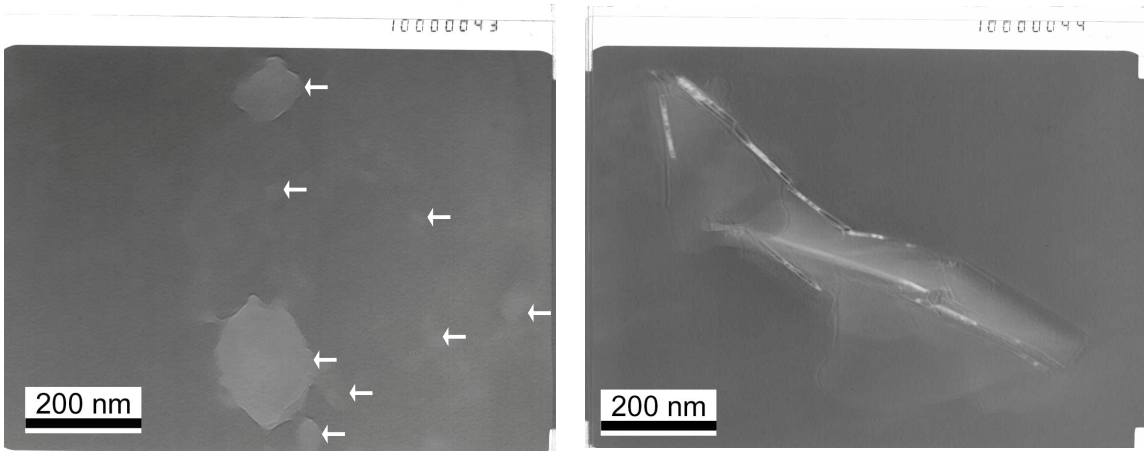

Figure 3. Transmission Electron Micrograph of Exfoliated Graphite Particles in an Epoxy Matrix. These ultramicrotomed sections are ~50nm thick. The left image shows individual platelets and the right image shows a platelet that has been folded over on itself.

Figure 3 is the TEM image of the composite. This TEM image shows some of the graphite platelets are sub-micron level in size. This picture is the first one that shows nanometer size graphite platelets dispersed in a polymer matrix. The adjacent TEM image also shows that the platelets have folded over on themselves indicating that the process has to be improved. Also note that not all platelets are pulverized into the sub-micron level.

DMA measurements were conducted in the temperature range of 30~120ºC. Figures 4 and 5 show that Tg (glass transition temperature) and density of the graphite platelet nanocomposite and the reference neat epoxy resin are almost the same. The storage moduli at 30ºC (below the Tg of the matrix) and 110°C (above Tg) were investigated.

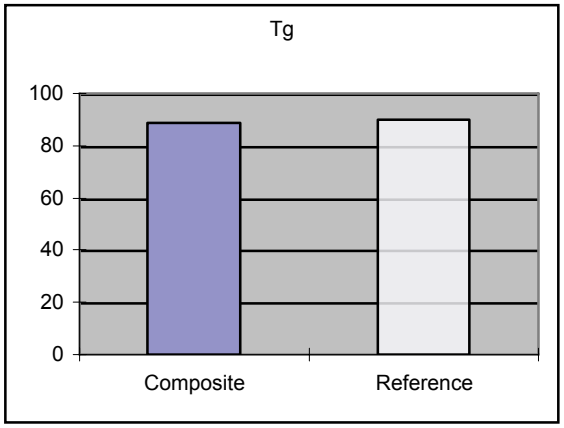

Figure 4. Tg of GraphiteŠEpoxy Nanocomposite.

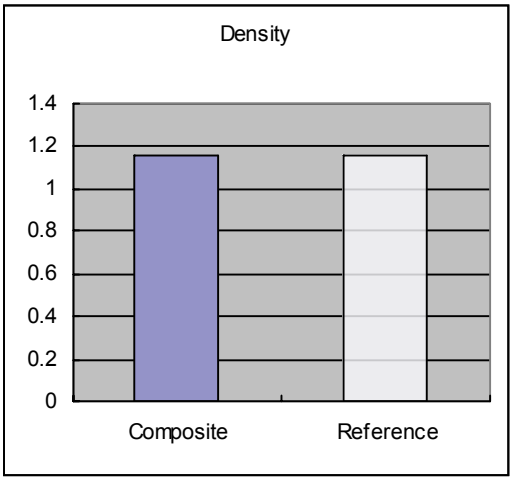

Figure 5. Density of Graphite-Epoxy Nanocomposite.

Figures 5 & 6 show the DMA results. Composite materials with 1wt% graphite showed about 15% improvement in storage modulus at 30ºC and 55% at 110°C compared to the matrix material. XRD data revealed that some of the graphite platelets are segregated at the bottom of the composite and these platelets are not exfoliated well while most of the graphite platelets dispersed in the matrix are exfoliated. If a more efficient exfoliation method can be achieved, much better mechanical properties would be expected

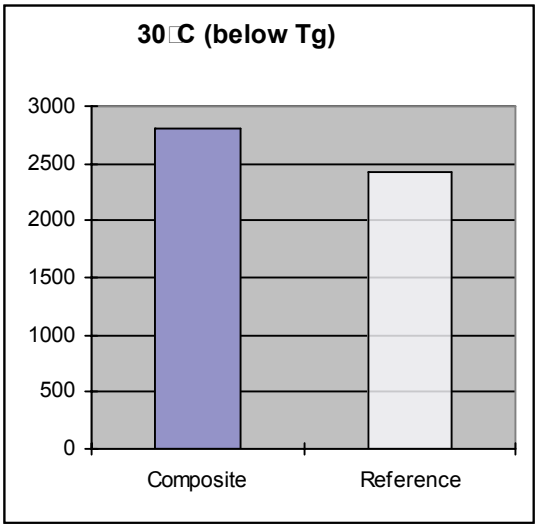

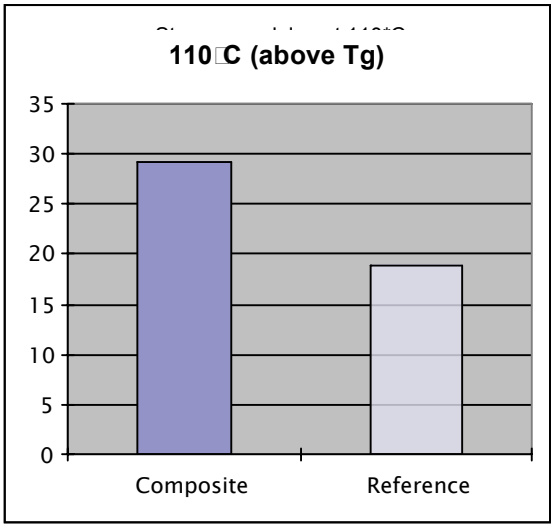

Figures 6 & 7. Storage Modulus of Graphite-Epoxy Nanocomposite below and above the Tg.

The modulus of the reference epoxy is measured as 2544 MPa and that of 1wt% graphite-reinforced composite is 2701 MPa. Assuming that the density of graphite is 1.85g/cc and that of the epoxy is 1.3g/cc, the volume fraction of graphite in this system is calculated to be 0.7%. With the assumption of perfect bonding and perfect alignment in one direction, the (parallel) rule of mixtures gives the upper bound of the composite modulus if it was composed of unidirectional fibers. Using this theory, the modulus of the graphite nanoreinforcement in this composite sample can be estimated as 227 GPa. By comparing this value to the Young's modulus of single crystal graphite (1060 GPa), we conclude that only a portion of the graphite flake is acting as a single basal plane and that more efficiency of exfoliation must be attained to reach the properties of single crystal graphite.

RESEARCH PLAN

Since graphite platelets have mechanical properties that are far superior to other nanoreinforcements and can rival those of the highest modulus carbon fibers, the incorporation of exfoliated graphite platelets into high performance epoxy and polyimide thermoset aerospace polymers will be emphasized. The key points to making graphite platelet nanocomposites are intercalation of polymers in graphite galleries and exfoliation of graphite platelets in a given polymer matrix. Furthermore the packing and orientation of the graphite platelets must be controlled in order to obtain the highest degree of mechanical, thermal and electrical properties in the polymer nanocomposite. Investigating these basic factors will make it possible to achieve nanocomposites, which can offer new properties and performance capabilities.

Graphite. Preliminary exfoliation and nanocomposite experiments were conducted with graphite procured from UCAR and the same material was used throughout this project. The graphite samples used in this research were Graphite Intercalate Compounds (GICs), which

were acid intercalated natural crystalline graphite flakes. The acid components consist of sulfuric and nitric acid. Nitric acid acts as an oxidizer while sulfuric acid acts as an intercalant. The acid intercalated graphite exhibits multiple stages, ranging from stage 1 to 5. The stage number indicates the number of graphene sheets between adjacent intercalated galleries. Upon heating, the intercalated acids become vapor and force layers apart, causing exfoliation of graphite layers. The sample grades used in this research are Grafguard^{TM} 160-50A, 160-50B, and 160-50N. Here "160" refers to the onset temperature at which intercalated acid begins to be released and exfoliation of the graphite occurs. "50" indicates the average size of the flakes is 50 mesh, which is 300 um. A, B, and N show the conditions of the sample surface, which are acidic, basic, and neutral. Acid, Basic and Neutralized graphites are readily available in 160 and 250 micron sizes.

Polymer Matrices. Because of previous successful achievements in fabricating nanocomposites, graphite-epoxy systems are appropriate as a standard sample. A baseline epoxy (diglycidyl ether of bisphenol-A) cured with a primary amine will be used as the matrix. This system has been shown in previous work to be a good model for high performance epoxy systems.

Dispersion. One major obstacle that has to be overcome in graphite platelet nanocomposites is to achieve individual particle dispersion in the polymer matrix. Spontaneous exfoliation cannot take place in typical highly viscous polymers. The application of shear in order to assist in the displacement of graphite sheets with respect to each other and to aid in their dispersion in the polymer matrix is a necessity. We intend to use Banbury mixing combined with the application of heat to achieve the dispersion degree necessary

Characterization of Intercalation. The degree of intercalation of monomers or polymers are an index of adhesion. Thus, model composites will be fabricated and the degree of intercalation will be investigated by X-ray diffraction of d_{001} plane of graphite and TEM (Transmission Electron Microscopy) observation of ultramicrotomed sections.

Surface Chemistry of the Interface. Since the factors that control the penetration of polymer chains into graphite galleries and exfoliation of graphite in a matrix polymer are unclear, this research focuses on evaluation of surface chemistry of the interface of nanocomposites which have been fabricated successfully.. *The chemical composition of the reinforcements and matrix polymers will be determined by XPS and FT-IR.*

Thermomechanical Properties. To control and maximize the properties of the composite, and to establish the relation between adhesion and composite properties the thermal and mechanical properties of nanocomposites will be evaluated. DMA (Dynamic Mechanical Analyses) will give both thermal (glass transition temperature) and mechanical (storage modulus) properties. Tensile strength and modulus will be measured by standard ASTM method.

Interfacial Shear Stress. The adhesion (i.e. interfacial shear strength) of the platelets in a matrix can be estimated by using an experimentally obtained Young's modulus and Eshelby equivalent inclusions method.

Alignment. Theoretically it is very clear that the ability to orient the exfoliated graphite platelets parallel to each other can produce a very large increase in mechanical properties (e.g. modulus), as well as achieving a low percolation threshold for improved thermal and electrical properties. Previous research in our group has resulted in the ability to align conductive and non-conductive

fibers in polymers with the application of external electric fields. We will be pursuing this approach coupled with the application of shear to increase the degree of platelet alignment.

This research program utilized an iterative process in order to understand and optimize the surface treatment, adhesion and composite properties. The ***FLOW CHART*** for the experimental plan is shown in Figure 8.

Summary. The concept of nanoreinforcements for composites was first introduced in the 80's, but so far, inorganic clay platelets have been the sole nanoreinforcement investigated. This research is directed at developing the ability to create nanographite platelets as an alternative to clays. Graphite nanoplatelets have a modulus at least ten times greater than that of clay, and the material is both thermally and electrically conductive. Key points for fabricating good graphite-polymer nanocomposites are intercalation of polymers into graphite galleries and exfoliation of graphite platelets in the matrix polymer. These phenomena are considered to be related to the adhesion condition between reinforcements and matrix, but success has been limited to a few cases and the basic factors that control these phenomena are unclear so that the maximum properties of the composite may not have been achieved.

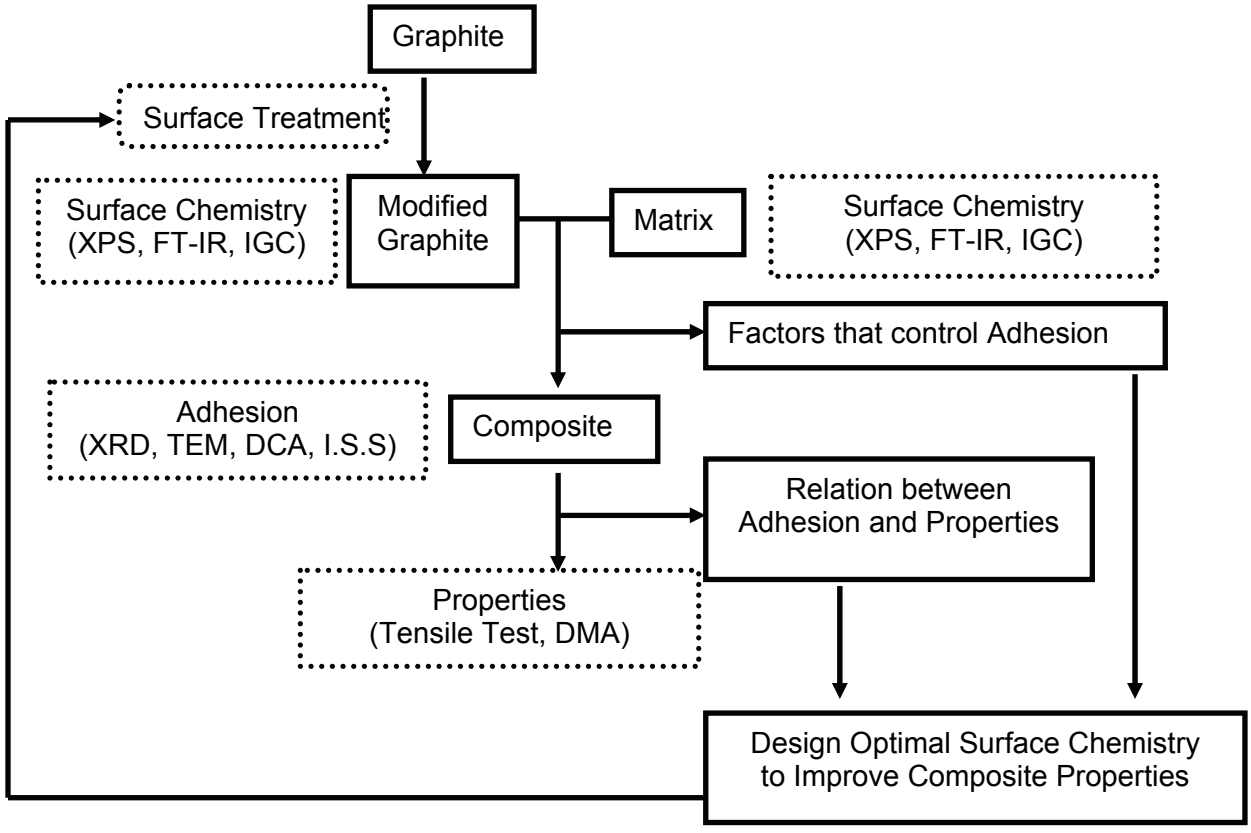

Figure 8. Flow Chart of the Experimental Pan

RESULTS

Exfoliation of Intercalated Graphite. Thermogravimetric analysis (TGA) at a rate of 20 ºC per minute revealed that initial expansion occurs around 160ºC, but most of it occurs in the range of 250 to 350 ºC [**Figure 9**]. The amount of acid intercalated in GICs was 21 to 25 wt%. During the expansion process, a graphite flake expands 100 to 1000 times in c-axis direction and makes a worm-like shape with flakes attached together [**Figure 10**]. This is called expanded graphite. Since 160-50A has the largest amount of acid and shows the highest degree of expansion, this research used 160-50A as the starting material.

Two factors affect the degree of expansion: temperature and the size of the GICs. To investigate the effect of temperature, 4g samples of 160-50A were exfoliated at 300, 400, 500, 600, 700, 800, 900, or 1000ºC for 3 min. **Figure 11** shows the image of the expanded graphite

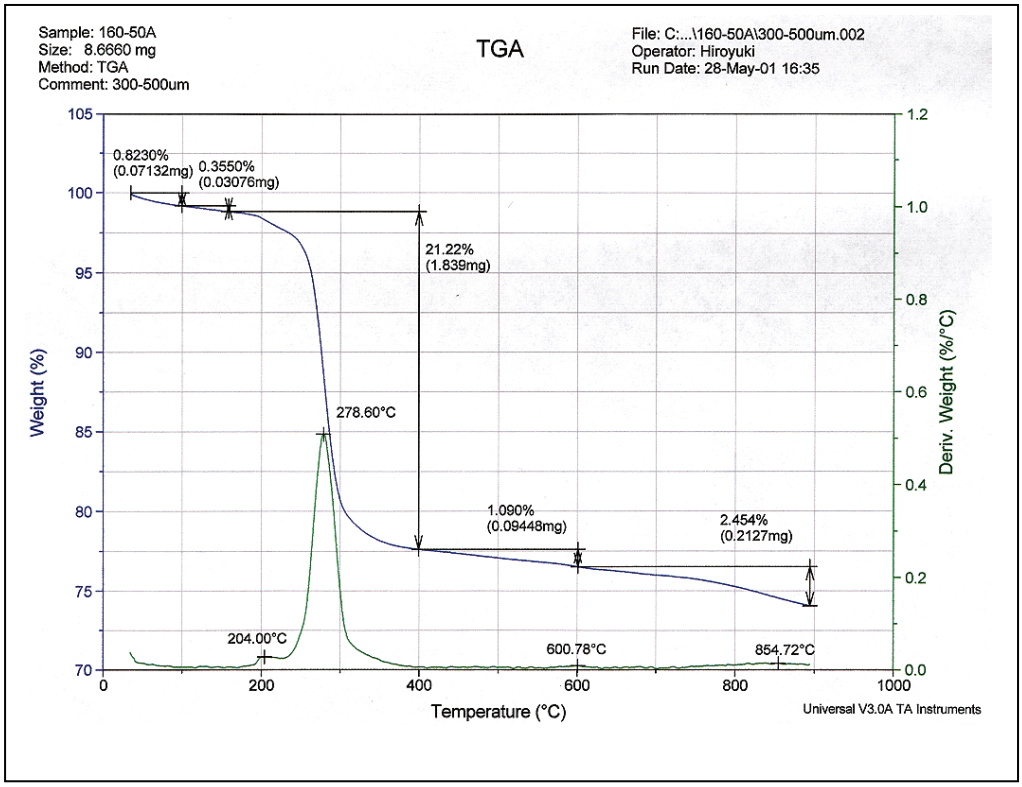

Figure 9. TGA Data of Acid Intercalated Graphite

samples after the treatment. This image reveals that the degree of expansion increased as temperature increased up to 600ºC, then it reached a plateau beyond that temperature. Thus, it is concluded that the temperature of 600ºC or higher is required to achieve the maximum degree of expansion. This also agrees with literature citations which indicate that temperatures above 800ºC were used to expand acid intercalated graphite platelets.

To investigate the effect of size, 160-50A flakes were sieved into different size categories, which are less than 25um, 25 to 75um, 75 to 106um, 106 to 180um, 180 to 300um, 300 to 500 um, and over 500 um. 0.1 g of each was placed in a crucible and expanded at 900 ºC for 5 min at the same time in the same furnace. **Figure 12** shows the image of these expanded graphites after the heat treatment. The larger the sample size, the larger the degree of expansion. This is because when the size of the flake is small the vaporized acid intercalate escapes from the edge rather than pushing the layers apart,. Also TGA data revealed that the smaller graphite has less acid intercalates (**Figure 13**). This implies that acid can vaporize slowly under ambient

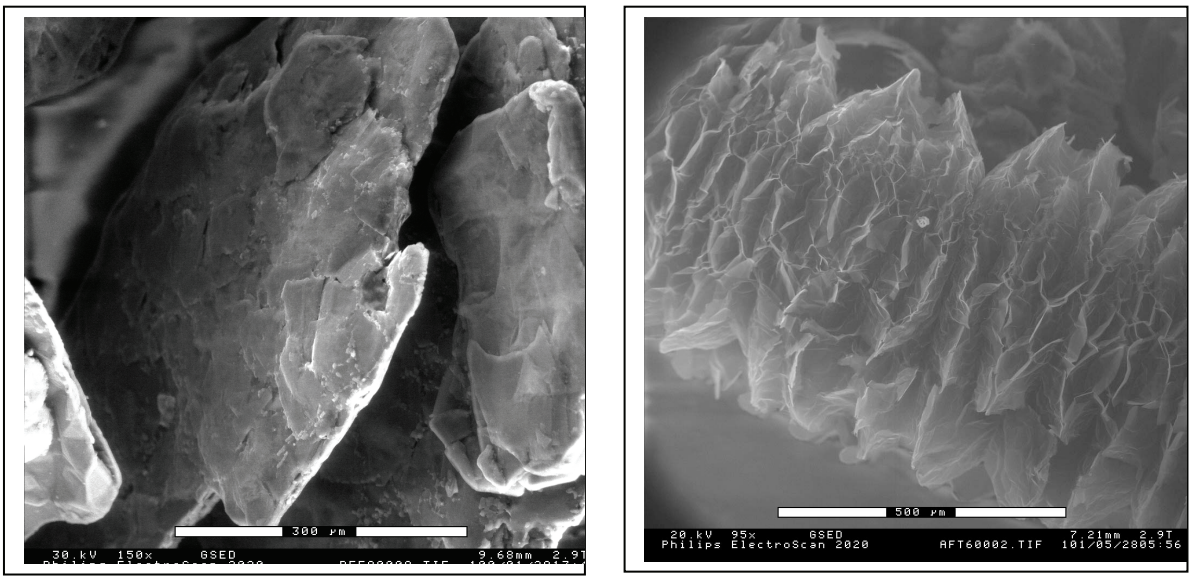

Figure 10. ESEM images of as-received 160-50A (left) and expanded graphite at 900ºC (right). (Scale = 500 um)

Figure 11. The Effect of Temperature on Degree of Expansion

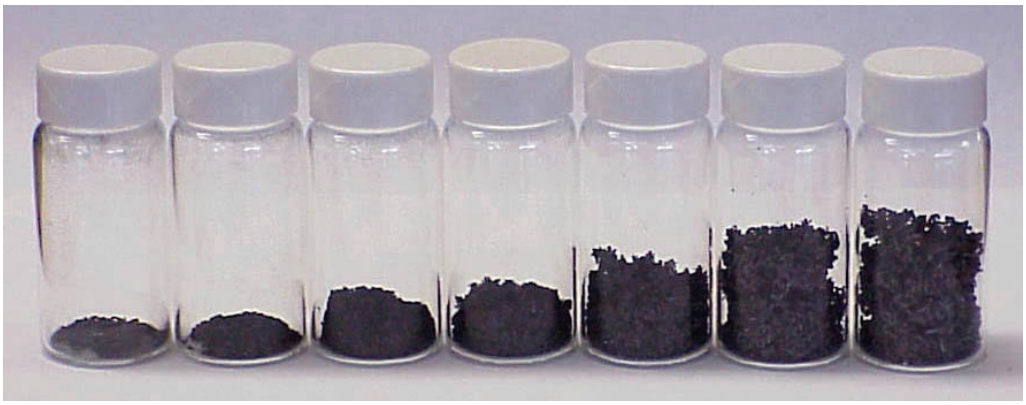

0-25um 25-75um 75-106um 106-180um 180-300um 300-500um +500um

Figure 12. The Effect of Size on Degree of Expansion (at 900ºC.)

conditions. Graphite flakes of 75 um or larger size show good expansion, and those of 180 um or larger show the maximum expansion.

Microwave (MW) processing has many advantages over conventional heating such as less energy consumption, speed, homogeneous and simultaneous heating throughout the whole sample, and higher process capacity. Because of these advantages, the microwave process often offers considerable cost reduction. Graphite material has many pi electrons, which can move in response to an electromagnetic field., leading to rapid heating of graphite materials. The temperature can reach a few hundred degrees Celsius within a few seconds. Thus, the microwave process can provide an alternative method to expand graphite-intercalated compounds. To demonstrate this, 2 g of GIC sample was put in a beaker and microwaved at 900 W for 5 seconds. The frequency of the microwave was 2.45 GHz.

Figure 14 shows the d002 peak of as-received GIC, heat exfoliated graphite (900º, 3min), and microwave exfoliated graphite (1040W, 3min). The peak corresponding to the d002 plane of

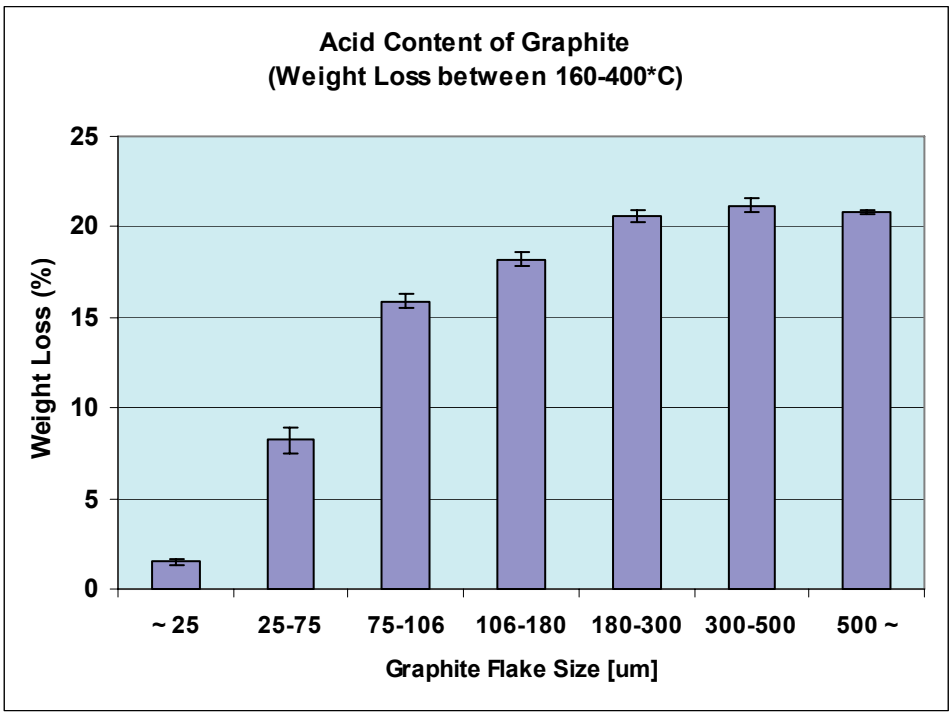

Figure 13. The Effect of Size on the Amount of Intercalant

the as-received 160-50A samples is large and sharp (**Figure 14A,** d002 = 24858 cps), while that of heat exfoliated graphite shows a lot smaller peak (**Figure 14B,** d002 = 163 cps), suggesting the most of the layered structure was destroyed because of the expansion. The d002 peak of the microwave exfoliated graphite became even smaller (**Figure 14C,** d002 = 62 cps), meaning the microwave process produces a greater degree of exfoliation than rapid oven heating. This is also confirmed by BET surface area measurement. The surface area of microwave exfoliated graphite samples reached 100m^2/g, which is more than 4 times larger than that of heat exfoliated samples (25m^2/g). The surface area for heat exfoliated graphite agrees well with literature values, which are in the range of 20-40m^2/g. The thickness of heat and microwave exfoliated graphite flakes was calculated based on the surface area data. the apparent thickness of heat exfoliated graphite was around 45nm while that of microwave exfoliated graphite was 10 nm. This result agrees well with the transmission electron microscope (TEM) images of microwave exfoliated graphite platelets in **Figure 15**. Thus, it is concluded that a microwave process gives a better degree of exfoliation of GIC, resulting in highly exfoliated graphite nanoplatelets with surface areas of above 100m^2/g and thicknesses of 10nm or less.

(A)

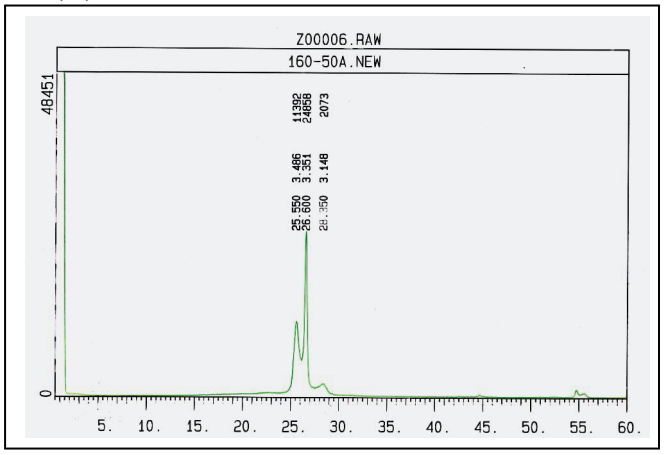

(B)

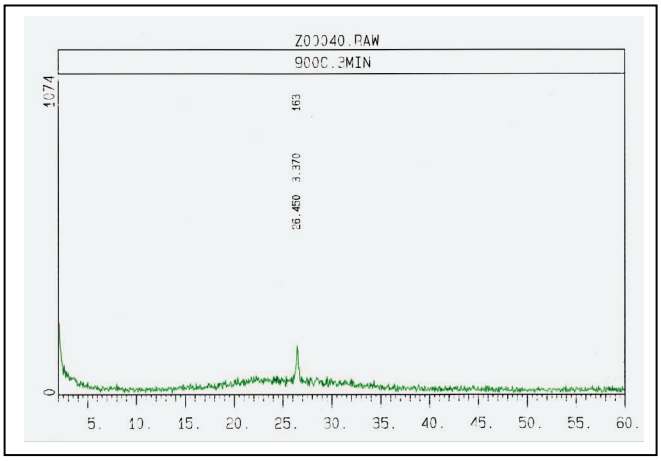

(C)

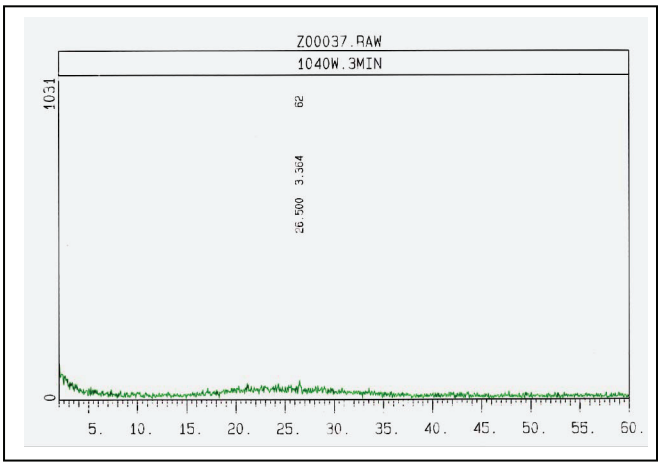

Figure 14. XRD curves of Graphite Samples. (A) As-received Graphite, (B) Expanded by Heating, 900ºC for 3min. (C) Expanded by Microwave, 1040W for 3min.

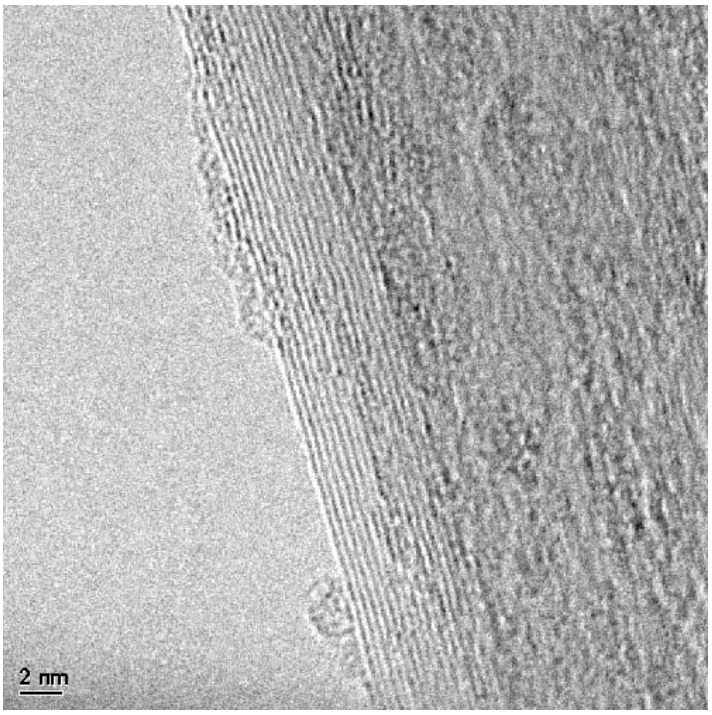

Figure 15. TEM images of MSU-Microwave Exfoliated Graphite Flake Scale Bar = 2 nm *(courtesy R. S. Ruoff, Northwestern University)*

Pulverization of Exfoliated Graphite. The worm-like graphite samples can be pulverized into small platelets by ultrasonic agitation, mechanical grinding, or other methods. 20 g of the expanded graphite sample was dispersed in 2 liters of acetone and pulverized by ultrasonic wave at 100W for 2 hours. **Figure 16** shows an environmental scanning electron microscope (ESEM) image and **Figure 17** shows the size distribution of the graphite particles after this treatment. The average size of this sample was 14.25 um. Smaller platelets can be obtained by ball milling, planetary milling, or other milling techniques. **Figure 18** shows the ESEM image of graphite platelets after 60 hours of ball milling. **Figure 19** shows the size distribution of that sample. The average size of the graphite becomes 0.86 um after this process. Thus it is possible to control the size of the exfoliated graphite nanoplatelet by controlling the pulverization and/or milling process. **Figure 20** shows a TEM image of exfoliated graphite after milling, which shows graphite platelets with diameters of a few-hundred nanometers. **Table 1** summarizes the dimensions of exfoliated and milled nanographites.

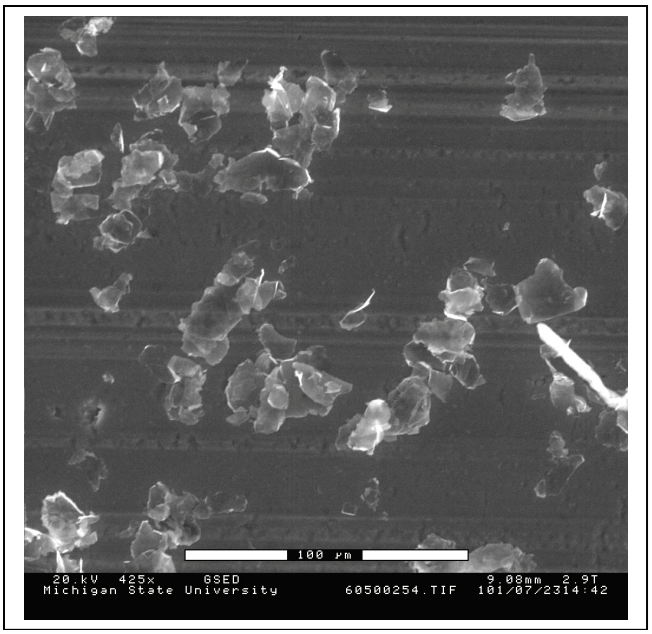

Figure 16. ESEM image of Graphite Platelets after Exfoliation and Pulverization (Scale Bar = 100um)

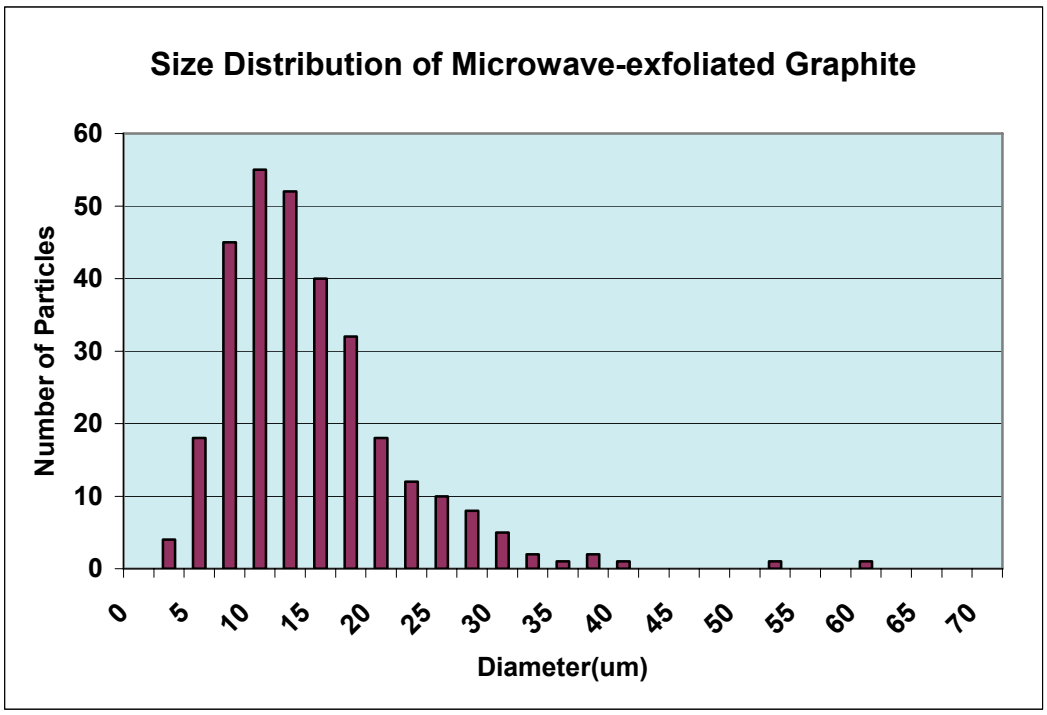

Figure 17. Size Distribution of Graphite Particle after Exfoliation and Pulverization by Ultrasonic Processor, Average Size = 14.25 um (Standard Deviation = 7.53

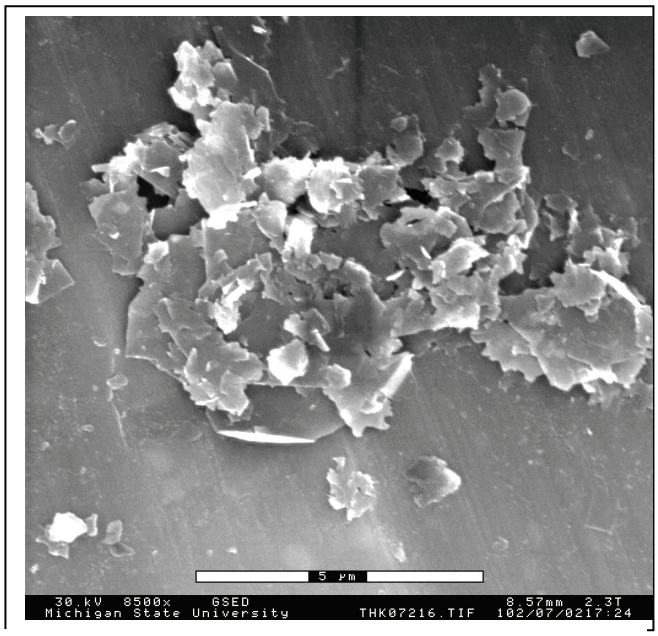

Figure 18. ESEM image of Graphite Fakes after Ball Milling (Scale Bar = 5um)

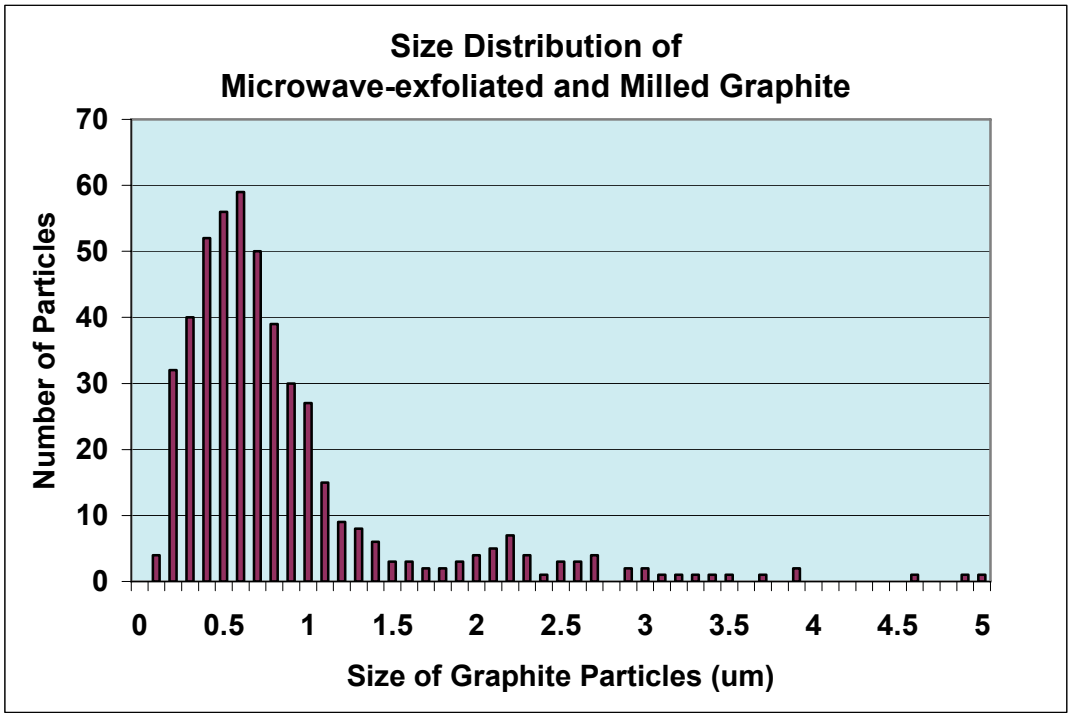

Figure 19. Size Distribution of Graphite Particle after Ball Milling (60 hr)
Average Size = 0.86 um (Standard Deviation = 0.73 um)

Table 1. Dimensions of Exfoliated graphite Nanoplatelets

	Exfoliation Process	Pulverization Process	Average Diameter (um)	Average Thickness (nm)	Surface Area (m^2/g)
Heat-exfoliated Graphite	Heat (900ºC)	Sonication	15	97	10.5
Heat-exfoliated and milled graphite	Heat (900ºC)	Sonication + ball milling	1.1	48	24
Microwave-exfoliated Graphite	Microwave (1300 W)	Sonication	15	10	105
Microwave-exfoliated and milled Graphite	Microwave (1300 W)	Sonication + ball milling	0.86	11	94

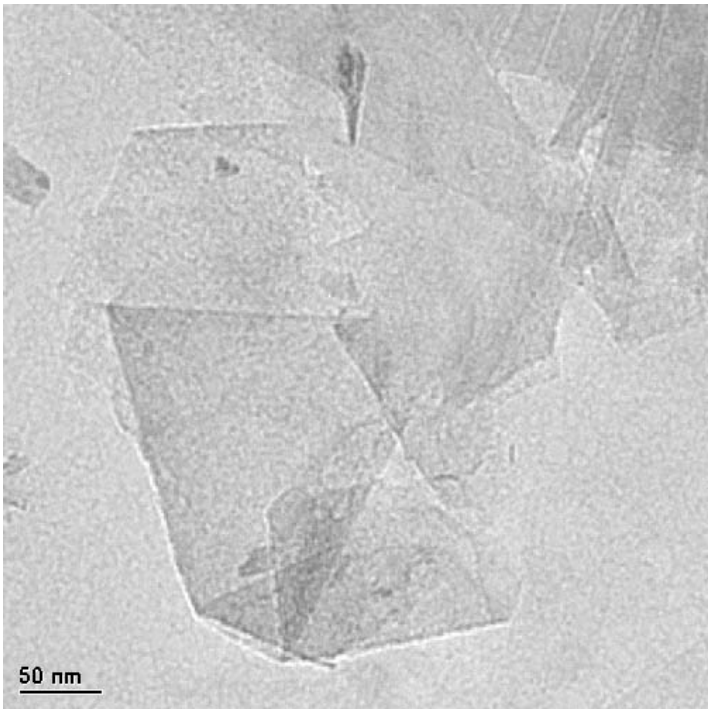

Figure 20. TEM images of Graphite Fakes after Ball Milling
Scale Bar = 50 nm (courtesy R. S. Ruoff, Northwestern University)

Surface chemistry of exfoliated and milled graphite samples was investigated with XPS. X-Ray Photoelectron Spectroscopy (XPS) was obtained from a Physical Electronics PHI 5400 ESCA system. A non-monochromatic Mg source (with a $K_{\square 1,2}$ wavelength at 1253.6 eV) was used with a take-off angle of 45 degrees. Data were collected by a multi-channel detector with an Omni VI lens assembly. The instrument was operated with a pass energy of 93.90 eV for survey scans and 29.35 eV for regional scans. All peaks were referenced to adventitious carbon at 284.6 eV. Semi quantitative atomic concentrations were calculated using pre-determined sensitivity factors. XPS samples were prepared by applying the graphite directly to double side copper tape on a stainless steel stub. Five to seven data points were collected and the average values were calculated. When a sample contained contaminates such as Zr, Si, and Al, the oxygen content of the sample was recalculated assuming these contaminates were ZrO_2, SiO_2, and $AlO_{1.5}$.

Based on these data, the ratio of oxygen/carbon (O/C), nitrogen/carbon (N/C), and sulfur/carbon (S/C) were calculated. The first two indicate the presence of functional groups which contain oxygen or nitrogen. The S/C ratio indicates the existence of sulfuric acid, which was intercalated into the as-received graphite platelets **Table 2** shows the XPS data while **Figure 21** shows the O/C, N/C, and S/C ratios. These data revealed that the diameter affects the functionality of graphite platelets while thickness does not. Calculations show that the edge area of flake materials increases significantly when the diameter becomes small, while it is affected very little by thickness of the platelets, (**Figure 22**). This supports the XPS results. Thus, it is concluded that the graphite platelets with smaller diameter have more functional groups than those with larger diameters. Also the results revealed that these materials have no nitrogen or sulfur, indicating the acid content has completely removed from the nanographite samples.

Table 2. XPS Data of Heat Treated and Microwave Treated Exfoliated Graphite Samples without Surface Treatment

	C	O	N	S	Zr	Na	Si	Al	O*	O/C
Heat-exfoliated Gr.	96.87	3.13	0.00	0.00	0.00	0.00	0.00	0.00	3.13	0.0324
Heat and Milled Gr.	93.50	6.14	0.00	0.00	0.22	0.00	0.17	0.00	5.37	0.0575
MW-exfoliated Gr.	96.79	3.21	0.00	0.00	0.00	0.00	0.00	0.00	3.21	0.0332
MW and Milled Gr.	91.17	8.02	0.00	0.00	0.81	0.00	0.00	0.00	6.41	0.0703

O* is the adjusted oxygen value

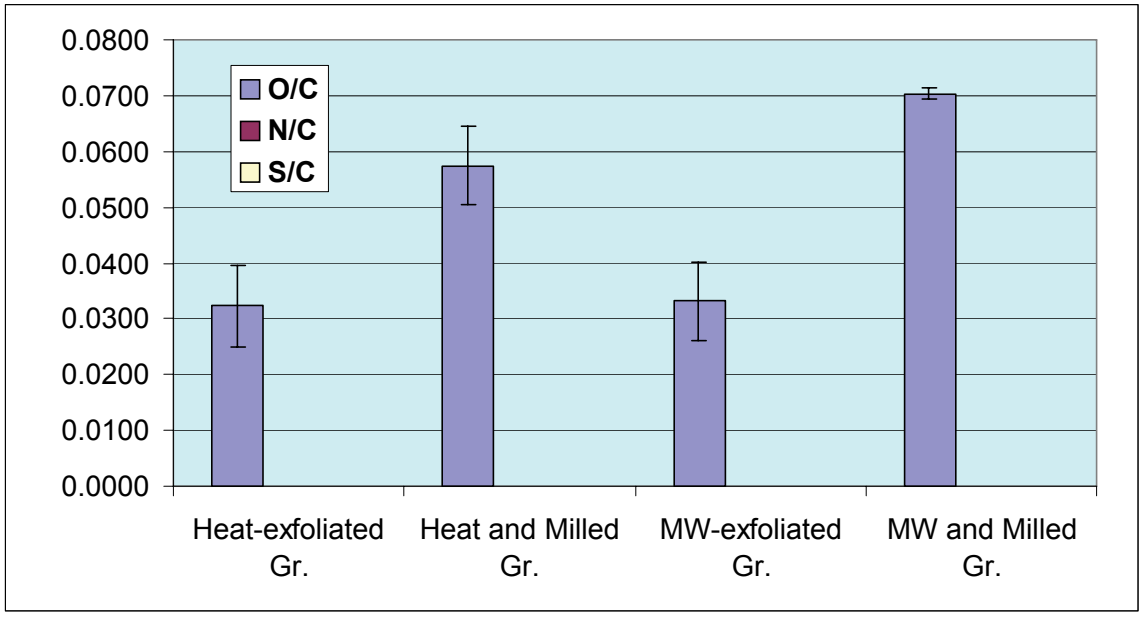

Figure 21. Surface Chemistry of Exfoliated Graphite Samples

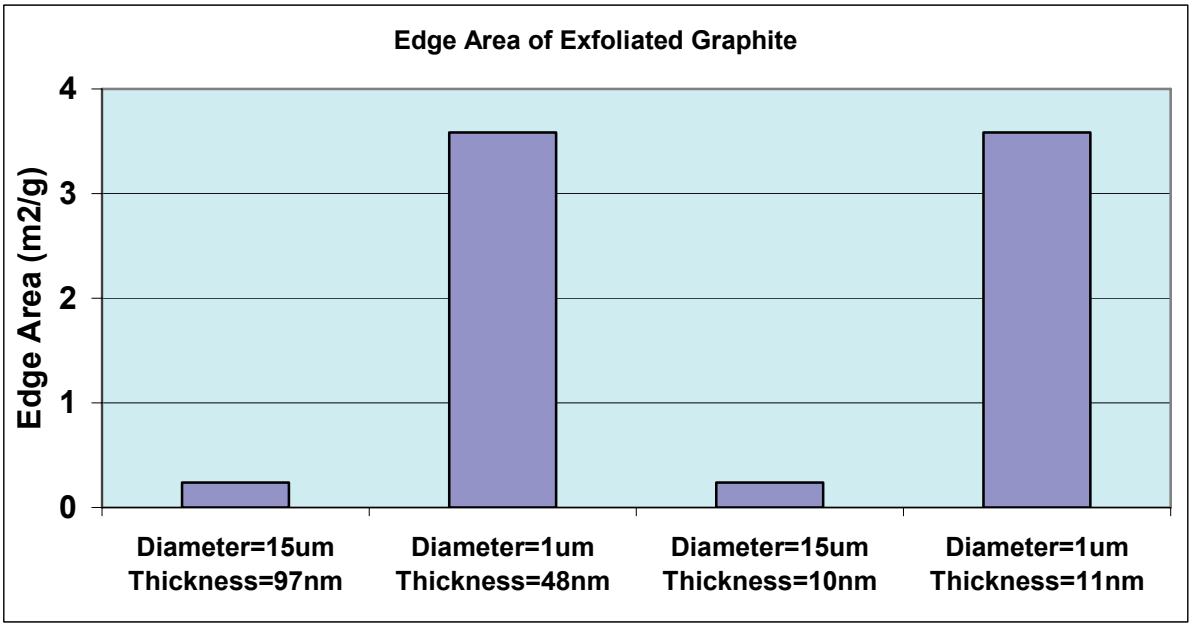

Figure 22. Theoretically Calculated Edge Area of Exfoliated Graphite Samples

A non-linear least square curve fitting routine was used to interpret the carbon, nitrogen, and oxygen peaks into functional groups, which exist on graphite samples. First, preliminary fitting for O1s curves was made and the ratio of two types of oxygen was determined. Then the carbon C1s and N1s curve fittings were made to separate these curves into several functional group categories. An asymmetric Gaussian-Lorentzian mixed band shape proposed by Sherwood *et al.* [22,23] was used to fit the curves. Because of the graphitic nature of the graphite materials, an exponential tail feature was found necessary for C1s 284.4ev curve. These curve-fitting routines have been developed based on extensive XPS work in our laboratory and the model proposed by Sherwood *et al.* [23,24,25]. The combination of O1s, N1s, and C1s curve fittings were used to determine the types and amount of functional groups, which existed on the reinforcements. It revealed that the graphite platelets with smaller diameters have more hydroxyl and ether groups than those with larger diameters do, but the amount of carboxyl groups was almost the same for all of these graphite platelets.

SURFACE TREATMENTS

According to the XPS data of exfoliated graphite samples, these materials do not have enough functional groups on their surfaces to interact well with polymer matrices. To improve the surface condition of exfoliated graphite samples, various surface treatments were applied on the microwave exfoliated and milled graphite nanoplatelets and the surface condition was investigated by XPS. The treatments used were liquid oxidization by sulfuric acid, plasma treatment under oxygen, heating under ozone atmosphere, UV treatment under ozone atmosphere, amine grafting, and acrylamide polymerization. Each of the treatments is described below.

O_2 Plasma Treatment

Graphite nanoplatelets were dispersed on an aluminum foil and covered by a stainless steel mesh. Then the sample was treated by O2 plasma at an RF level of 50% (275W). After the first treatment, the sample was re-dispersed on the foil and the process was repeated 3 times. The total treatment time was 1 minute. The XPS data revealed that the O/C ratio increased in all cases, suggesting functional groups were introduced. Functional group analysis revealed that the O_2 plasma treatment introduced mainly hydroxyl and carbonyl groups. The hydroxyl groups could improve the surface condition.

Nitric Acid Treatment

Graphite nanoplatelets were dispersed in 69 % (weight) of nitric acid and heated at 115 ºC for 5 hours. The sample was then washed with distilled water and dried in a vacuum oven. The XPS data revealed that the O/C ratio was not increased as much as it was in the case of the O_2 Plasma treatment. Also functional group analysis showed little increase in functionality. Thus, it is concluded that the nitric acid treatment was not as effective as O_2 plasma treatment.

Ozone/Heat Treatment

Graphite nanoplatelets were dispersed in a petri dish and placed in an oven which was filled with ozone . (Concentration: 2000 ppm) Then the samples were heated at 80ºC for 20 min. During this time the sample was re-dispersed several times so that the all the graphite platelets were exposed to the ozone environment. XPS revealed that the O/C ratio was not increased after the treatment, suggesting that this treatment is not effective for these graphite materials. Functionality analysis supported this conclusion. This treatment could be effective for amorphous regions of graphite samples, but not for exfoliated graphite samples, which have highly crystalline structures.

UV/Ozone Treatment
Graphite nanoplatelets were packed in a quartz tube (ID: 22 mm, OD: 25 mm, Transparent to UV light down to a wavelength of 150 nm). The tube was filled with ozone (Concentration: 2000 ppm, Flow rate: 4.7 L/min) and rotated at 3 rpm. Then the samples were exposed to UV light for 5min. The O/C ratio was not increased after the treatment, suggesting this treatment was not effective for these graphite materials. Functionality analysis showed this process could introduce carboxyl groups, but not significantly. It is considered that this treatment is also effective for amorphous regions of graphite samples, but not for exfoliated graphite samples, which have highly crystalline structures.

TEPA Grafting Treatment
Graphite nanoplatelets were first treated with O_2 plasma to introduce carboxyl groups, then dispersed in tetraethylenepentamine (TEPA) and heated at 190ºC for 5 hours to graft TEPA by forming amide linkages [26,27]. The sample was washed with distilled water and methanol, then dried in a vacuum oven. The XPS data revealed the O/C ratio was not increased after the treatment, but nitrogen were introduced and the N/C ratio was increased significantly, suggesting many functional groups that include nitrogen were attached to the surface of the sample. Functionality analysis revealed that primary and secondary amines were the main functional groups introduced on the graphite surface; amide groups were also added. These functional groups can react with epoxy matrix and form covalent bonds. Thus, amine grafting treatment could improve the surface condition of the exfoliated graphite and potentially enhance the mechanical properties of composites filled with the reinforcements. TGA measurement showed about 1.56 wt% of organic content was introduced after the treatment.

Acrylamide Grafting Treatment
Graphite nanoplatelets were treated with O_2 plasma to introduce peroxide groups, which can initiate radical polymerization. Then the sample was dispersed in 1M acrylamide/benzene solution and heated at 80ºC for 5 hours to graft and polymerize acrylamide. The sample was washed with acetone and dried in a vacuum oven [28]. Both the O/C ratio and N/C ratios were increased significantly, suggesting many functional groups that include oxygen, nitrogen, or both were introduced. In fact, acrylamide grafting treatment gave the biggest increase in both oxygen and nitrogen contents. The functionality analysis revealed that amide groups were the main functional groups introduced; primary and secondary amines were also added. These functional groups can form covalent bonds with some polymers, including epoxies, and improve adhesion between the matrix and reinforcements. Thus, this treatment could offer very good improvements to the surface condition of the exfoliated graphite samples and enhance the mechanical properties of composites filled with the reinforcements. TGA analysis showed about 34 wt% of organic content was introduced after the treatment.

X-Ray Photoelectron Spectroscopy (XPS) was obtained from a Physical Electronics PHI 5400 ESCA system. A non-monochromatic Mg source (with a $K_{\alpha 1,2}$ wavelength at 1253.6 eV) was used with a take-off angle of 45 degrees. Data was collected by a multi-channel detector with an Omni VI lens assembly. The instrument was operated with a pass energy of 93.90 eV for survey scans and 29.35 eV for regional scans. All peaks were referenced to adventitious carbon at 284.6 eV. Semi quantitative atomic concentrations were calculated using pre-determined sensitivity factors. XPS samples were prepared by applying the graphite directly to double side copper tape on a stainless steel stub. Five to seven data points were collected and the average values were calculated. When a sample contained contaminates such as Zr, Si,, and Al, the oxygen content of the sample was recalculated assuming these contaminates were ZrO_2, SiO_2, and $AlO_{1.5}$. Based on these data, the ratio of oxygen/carbon (O/C), nitrogen/carbon (N/C), and sulfur/carbon (S/C) were calculated. The first two indicate the presence of functional

groups which contain oxygen or nitrogen. The S/C ratio indicates the existence of sulfuric acid, which was intercalated into the as-received graphite platelets. **Table 3** shows the results.

Table 3. XPS data of Exfoliated Graphite with Various Surface Treatments

MW Milled	C	O	N	Zr	O*	O/C	N/C
No Treatment	91.17	8.02	0.00	0.81	6.41	0.0703	0.0000
O2 Plasma	88.85	10.30	0.00	0.85	8.60	0.0968	0.0000
HNO3	92.27	6.93	0.00	0.61	5.72	0.0620	0.0000
O3/Heat	94.92	4.96	0.00	0.11	4.74	0.0499	0.0000
UV/O3	94.95	5.02	0.00	0.10	4.8233	0.0508	0.0000
TEPA	88.68	5.69	5.28	0.36	4.975	0.0561	0.0597
Acrylamide	71.41	16.59	11.86	0.14	16.32	0.2302	0.1701

The combination of O1s, N1s, and C1s curve fittings were used to determine the types and amount of functional groups, which existed on the reinforcements. **Table 4** and **Figure 23** summarize the results.

Table 4. Functional Group Analysis Data of Exfoliated Graphite with Various Surface Treatments

	-C-O-C-	-OH	-C=O	-COOH	-NH, -NH2	-CONH-, -CONH2	Oxidized amine
No Treatment	2.289	2.925	0.000	0.755	0.000	0.000	0.000
O2 Plasma	1.705	4.494	1.250	1.215	0.000	0.000	0.000
Nitric Acid	0.365	3.334	0.000	1.192	0.000	0.000	0.000
O3/Heat	1.387	2.290	0.322	0.796	0.000	0.000	0.000
UV/O3	0.228	2.674	0.000	1.234	0.000	0.000	0.000
Amine Grafting	0.705	0.391	0.935	1.154	1.859	0.741	0.350
Acrylamide	1.246	3.443	2.998	0.235	3.151	6.359	0.000

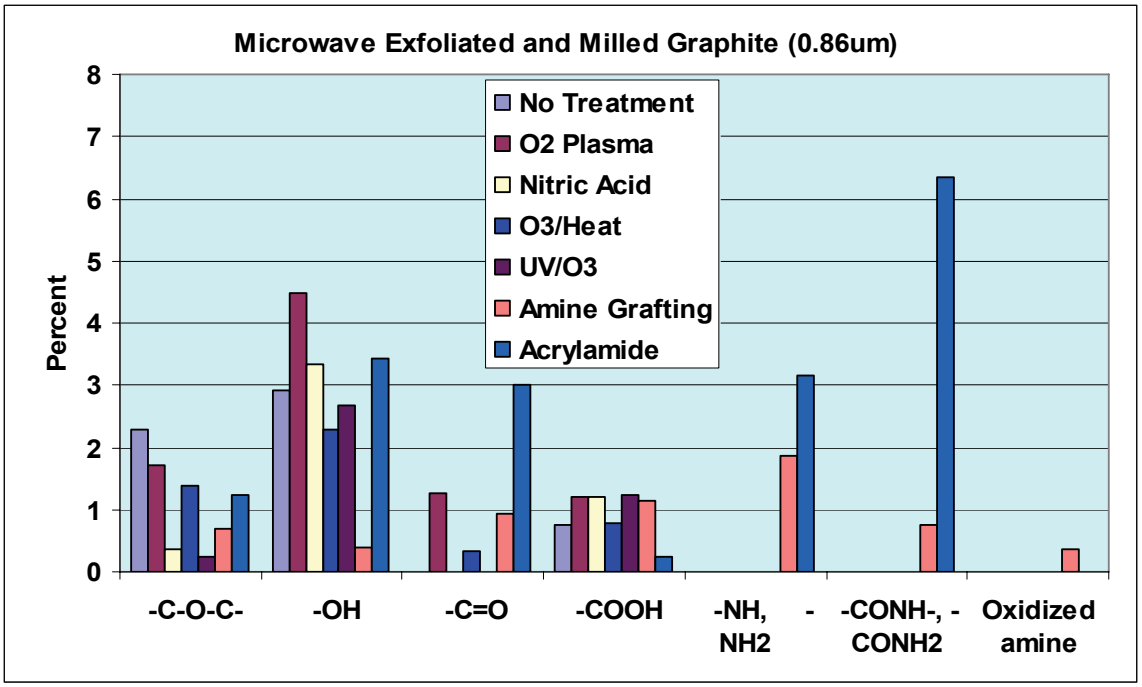

Figure 23. Functional Group Analysis Data of Exfoliated Graphite with Various Surface Treatments

Thermoset Composite Fabrication Epoxy was used as the matrix material. Diglycidyl ether of bisphenol A (Epon 828) was purchased from the Shell Chemical Co. Jeffamine T403 from Huntsman Petrochemical was used as the curing agent for this matrix system. The chemical structures of these materials are shown in **Figure 24**. The stoichiometry of these chemicals is 100 (DGEBA) to 45 (T403) by weight. The calculated amount of the reinforcement was added to DGEBA and mixed with the aid of an ultrasonic homogenizer for 5 to 10 minutes. Then the stoichiometric amount of Jeffamine T403 was added and mixed at room temperature. To avoid voids, a thorough outgassing process was applied before curing. The system was cured at 85ºC for 2 hours, followed by post curing at 150ºC for 2 hours. The volume fraction of carbon materials in composite samples was calculated assuming a density of graphite platelets of 2.0 g/cm^3. The densities of other carbon materials were obtained from their manufacturers. The density of the epoxy matrix was measured as 1.159 g/cm^3.

A. Epon 828

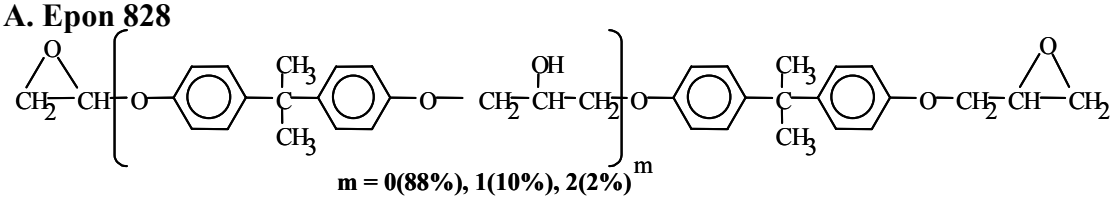

m = 0(88%), 1(10%), 2(2%)

Epoxide equivalent weight 185~192

B. Jeffamine T403

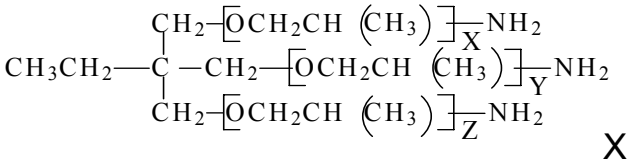

X + Y + Z = 5.3

Epoxide Equivalent Weight 185-192

Figure 24. Chemical structure of Diglycidyl ether of bisphenol A (A, Epon 828, Shell Chemical Co.) and Jeffamine T403 (B, Huntsman Petrochemical Co.)

Reinforcements for Comparison

Three commercially available carbon materials were used as comparison, which were PAN based carbon fiber (PANEX 33 MC Milled Carbon Fibers, Zoltek Co.), VGCF (Pyrograf III, PR-19 PS grade, Pyrograf Products, Inc.), and nanosize carbon black (KETJENBLACK EC-600 JD, , Akzo Novel Polymer Chemicals LLC). These materials were used as-received unless otherwise mentioned. **Table 5** shows the dimensional characteristics of these materials, while **Figure 25** shows SEM images of these materials. **Table 6** and **Table 7** along with **Figure 26** summarize the XPS and functional group analysis data of these materials.

Table 5. The Commercially Available Carbon Materials

	Average Length (um)	Average Diameter (nm)	Aspect Ratio	Surface Area (m^2/g)	Density (g/cm^2)
CF	175	7200	24.3	16	1.81
VGCF	50-100	150	333-666	25	2.0
Carbon Black		10-30	1	1400	1.8

Table 6. XPS data of Commercially Available Reinforcements

	C	O	N	S	Zr	Na	Si	Al	O*	O/C	N/C	S/C
CF	88.90	9.30	1.60	0.00	0.00	0.25	0.00	0.00	9.30	0.1046	0.0180	0.0000
VGCF	95.07	4.94	0.00	0.00	0.00	0.00	0.00	0.00	4.94	0.0520	0.0000	0.0000
CB	91.70	8.26	0.00	0.00	0.00	0.00	0.00	0.00	8.26	0.0901	0.0000	0.0000

Table 7. Functional group Data of Commercially Available Reinforcements

	-C-O-C-	-OH	-C=O	-COOH	-NH, -NH2	-CONH-, -CONH2	Oxidized amine
CF	1.586	2.964	0.457	1.013	0.553	1.347	0.000
VGCF	2.851	0.936	0.000	1.555	0.000	0.000	0.000
CB	4.026	0.846	0.000	3.794	0.000	0.000	0.000

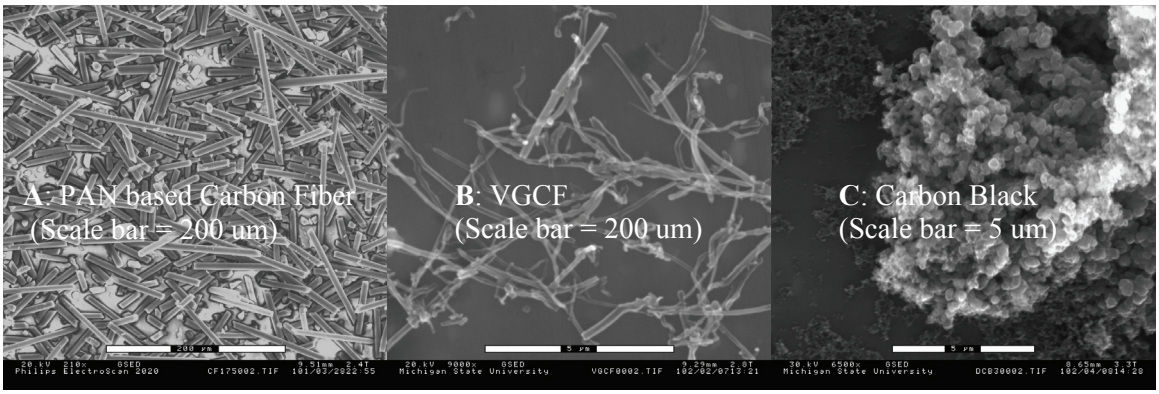

Figure 25. SEM of PAN based carbon fiber (A), VGCF (B), and carbon black (C).

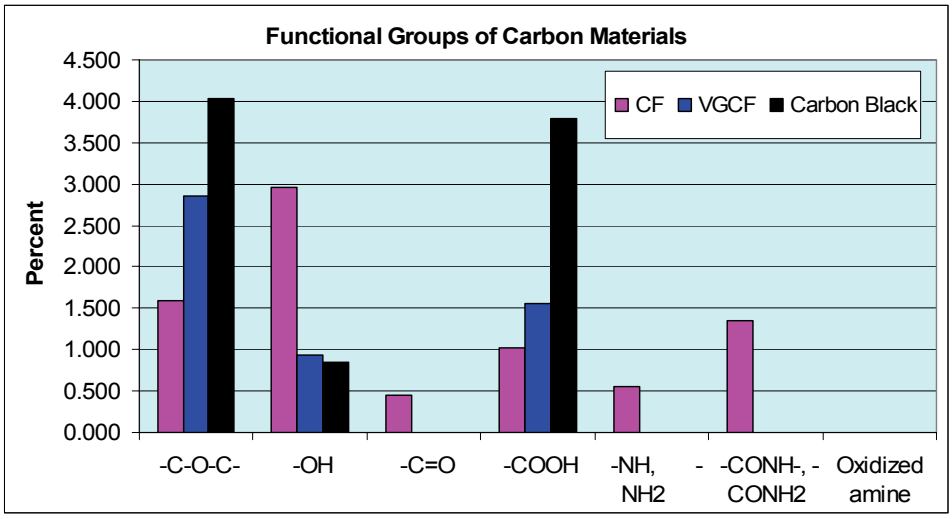

Figure 26. Functional Group Data of Commercially Available Reinforcements

Composite Flexural Mechanical Properties The flexural test was performed on a UTS testing machine [United Calibration Corp.] at room temperature following ASTM D790. The samples were made in a standard bar shape and polished carefully so that the thickness of the samples was constant throughout the samples. The final dimension of the bar samples was 60 x 12.5 x 3 mm. The test was performed at crosshead rate of 0.05 inches per minute.

Size effect

Composite samples with four different exfoliated graphite platelets were fabricated and the flexural properties are summarized in **Figure 27**. The composites filled with smaller graphite

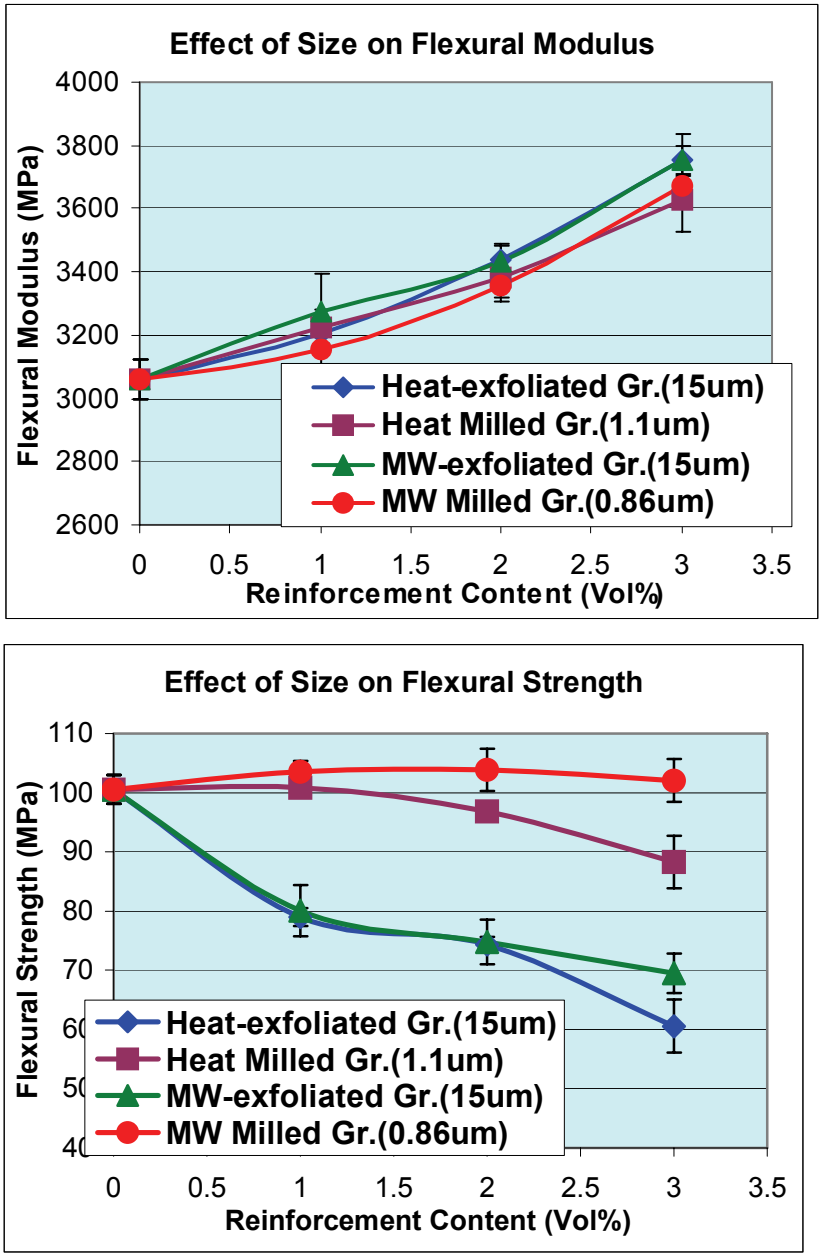

Figure 27. Effect of Size of Graphite Platelets on Flexural Properties

platelets showed better strength, implying those have better interactions with the matrix. These

results agree with the fact that smaller graphite platelets have larger edge area and higher functionalities than larger graphite platelets. Moduli were not affected by the size of graphite platelets. In theory, composites filled with fillers with larger aspect ratio should show a higher modulus, but the adhesion between fillers and matrix also affects the efficiency of stress transfer. These factors may compensate and resulted in almost the same modulus values in this case.

Effect of Surface Treatment

Various surface treatments were examined and three of them were considered to be good candidates for improving the surface chemistry of exfoliated graphite samples: O_2 plasma, amine grafting and acrylamide grafting. These three surface treatments were applied to the heat-exfoliated and milled graphite samples and epoxy composites were made. **Figure 28** shows the functionality of the surface treated graphite samples. The flexural properties of these samples were measured and summarized in **Figure 29**. Acrylamide grafting improved the properties the most, followed by the amine grafting treatment. O_2 plasma treatment did not improve the mechanical properties. These results suggest that both chemical interactions between amine functional groups on graphite and the epoxy matrix, and physical/mechanical interactions between grafted polymers/oligomers and matrix polymer play roles to enhance the flexural properties of the composite samples.

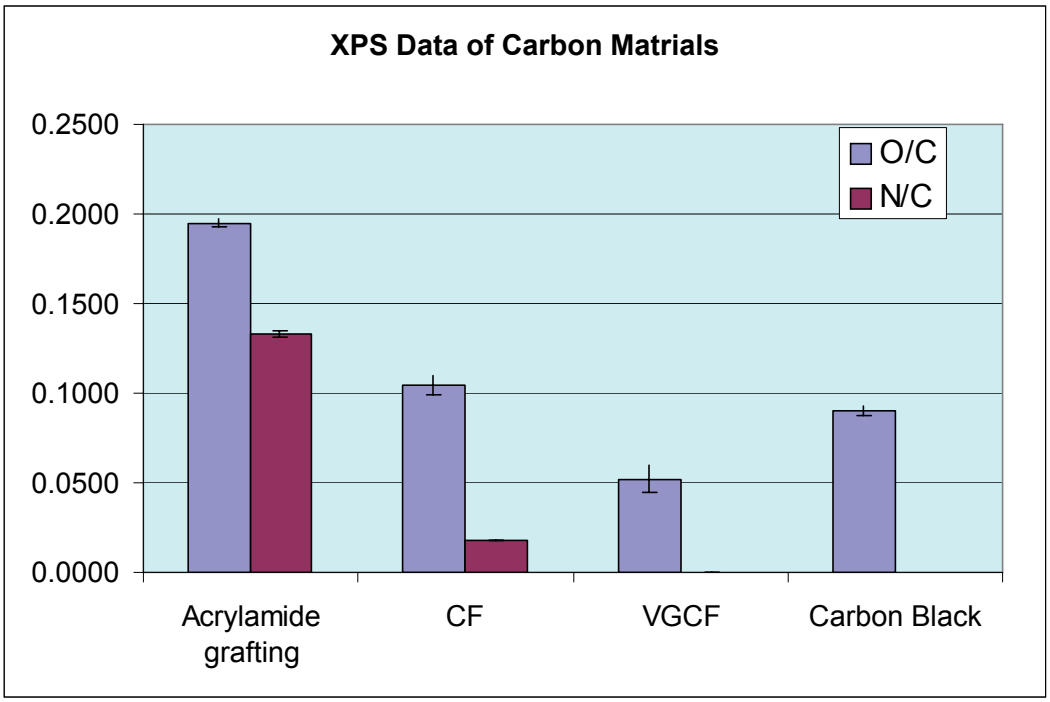

Figure 28. Surface Chemistry of Various Carbon Materials

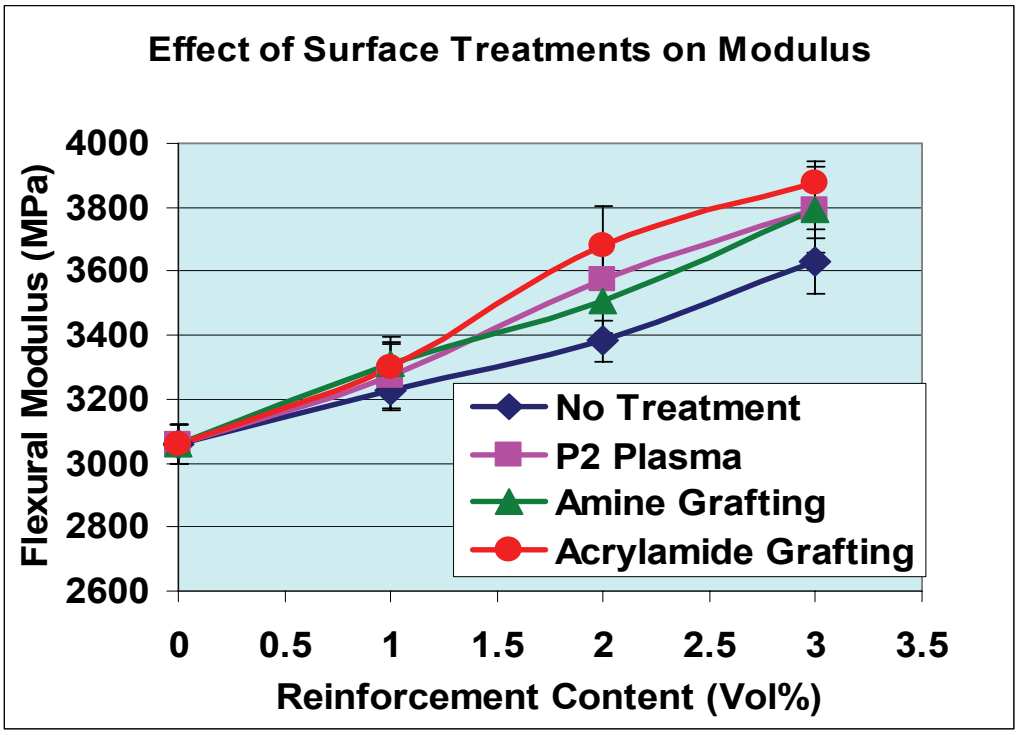

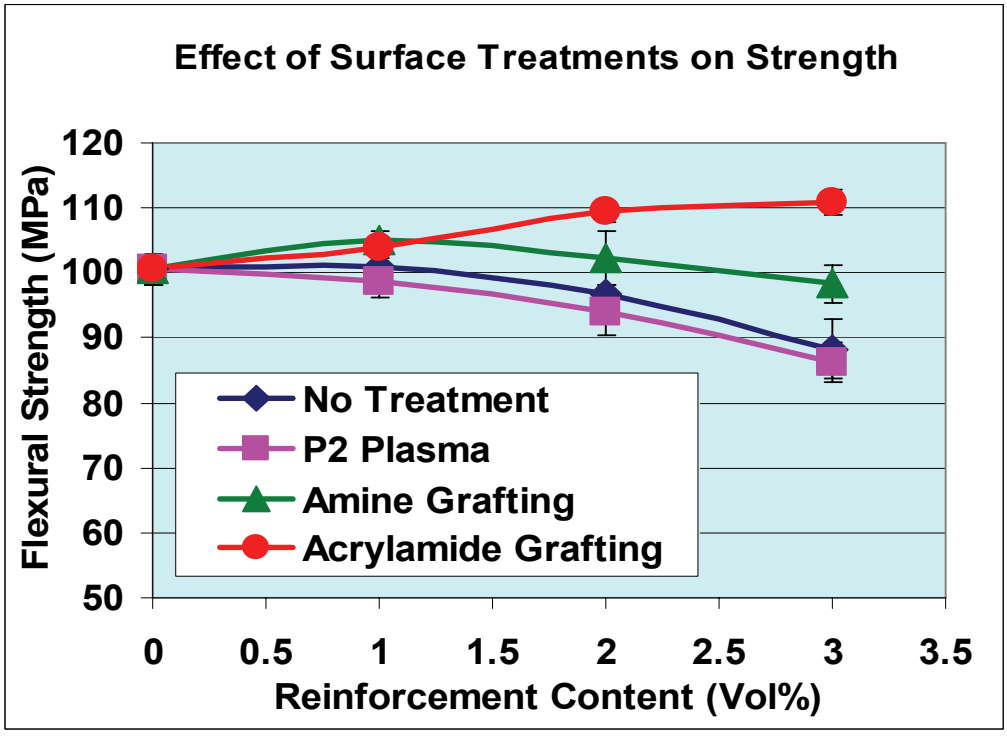

Figure 29. The Effect of Surface Treatments on Flexural Properties

Comparison of Exfoliated Graphite Platelets with Commercially Available Carbon Materials

Figure 30 shows the flexural modulus of epoxy composites reinforced with various carbon materials. The results showed the composites filled with acrylamide grafted xGnP-1 platelets showed higher modulus, implying those have better interactions with the matrix. In theory, composites filled with reinforcements with larger aspect ratios should have higher modulus, but

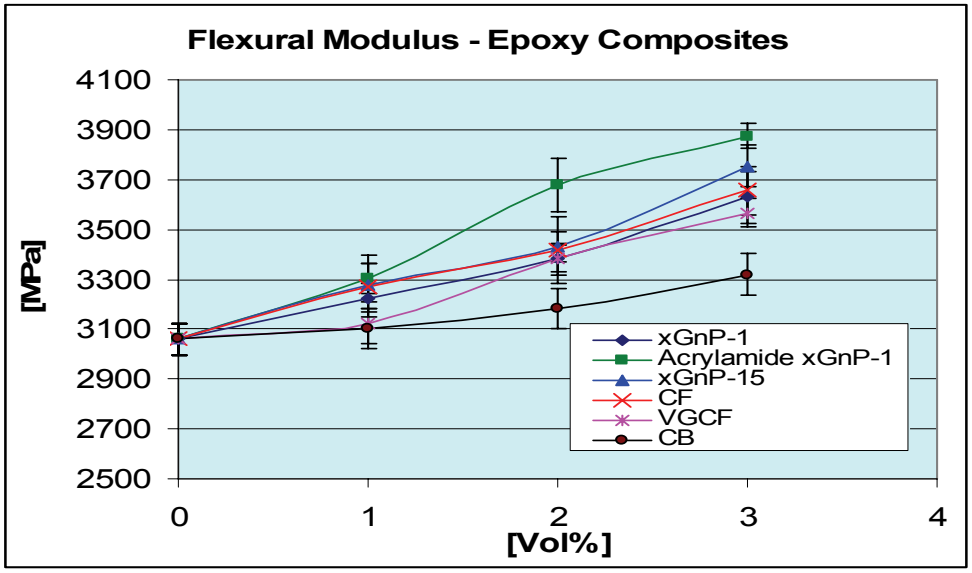

Figure 30. Flexural Modulus of Epoxy Composites

adhesion between fillers and matrix also affects the efficiency of stress transfer in the matrix

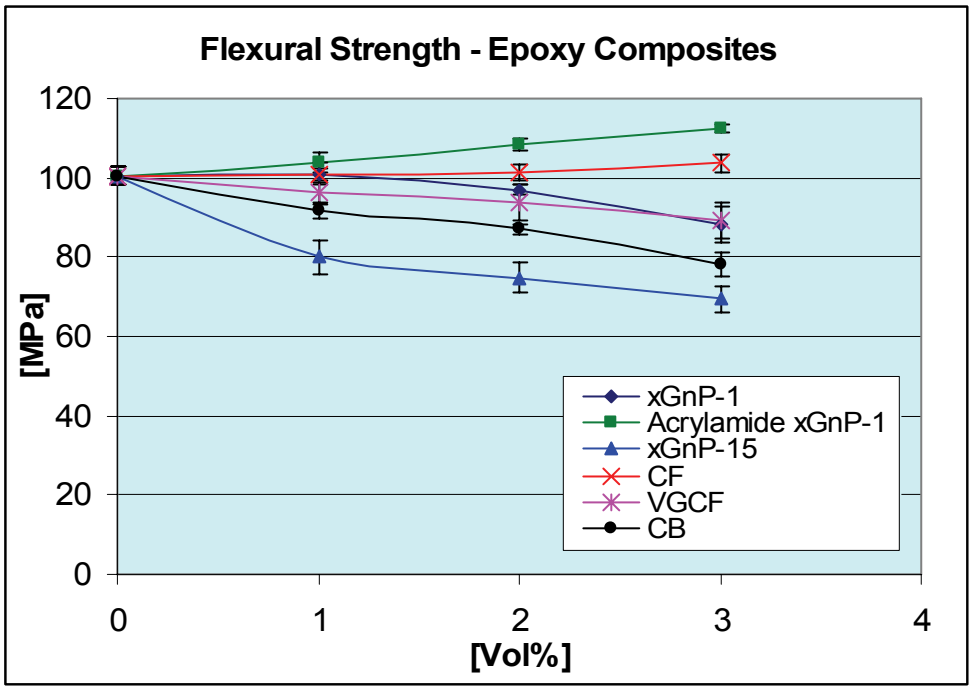

Figure 31. Flexural Strength of Epoxy Composites

system. According to XPS data, xGnP-1 has larger edge area and more functional groups than xGnP-15. This may give xGnP-1 better adhesion to epoxy and compensate the effect of aspect ratio. Also, acrylamide grafted xGnP-1 showed higher modulus than the commercially available carbon reinforcements. This proves that the exfoliated graphite nanoplatelets can be excellent reinforcements for polymer composites if appropriate surface treatments are applied. **Figure 31** shows the flexural strength of epoxy composites reinforced with various carbon materials. Composites reinforced with acrylamide grafted xGnP-1 platelets showed the highest strength, implying the surface treatment works really well in the epoxy system. This is reasonable because functionality data revealed that acrylamide grafted xGnP-1 has amine groups, which can react with epoxy resins and form covalent bonds. The adhesion can be improved significantly if the reinforcements are connected to the matrix through covalent bonds. Also, it should be noted that xGnP-1 showed higher strength than xGnP-15. This is because the exfoliated graphite nanoplatelets with smaller size have larger edge area and more functional groups, making them a better reinforcements.

Dynamic Mechanical Analysis (DMA)

Composite samples with 3 vol% of carbon reinforcements were fabricated and Tg was determined from the inflection point of the storage modulus curves. **Figure 32** shows that Tg was not affected by the carbon materials used. This result suggests that even though there were some chemical interactions between reinforcements and matrix, the proportion of the chemical interactions was so low that the chemical interaction did not affect the properties of the epoxy matrix. Also physical and mechanical interactions between matrix and reinforcements based on intercalation did not noticeably affect Tg.

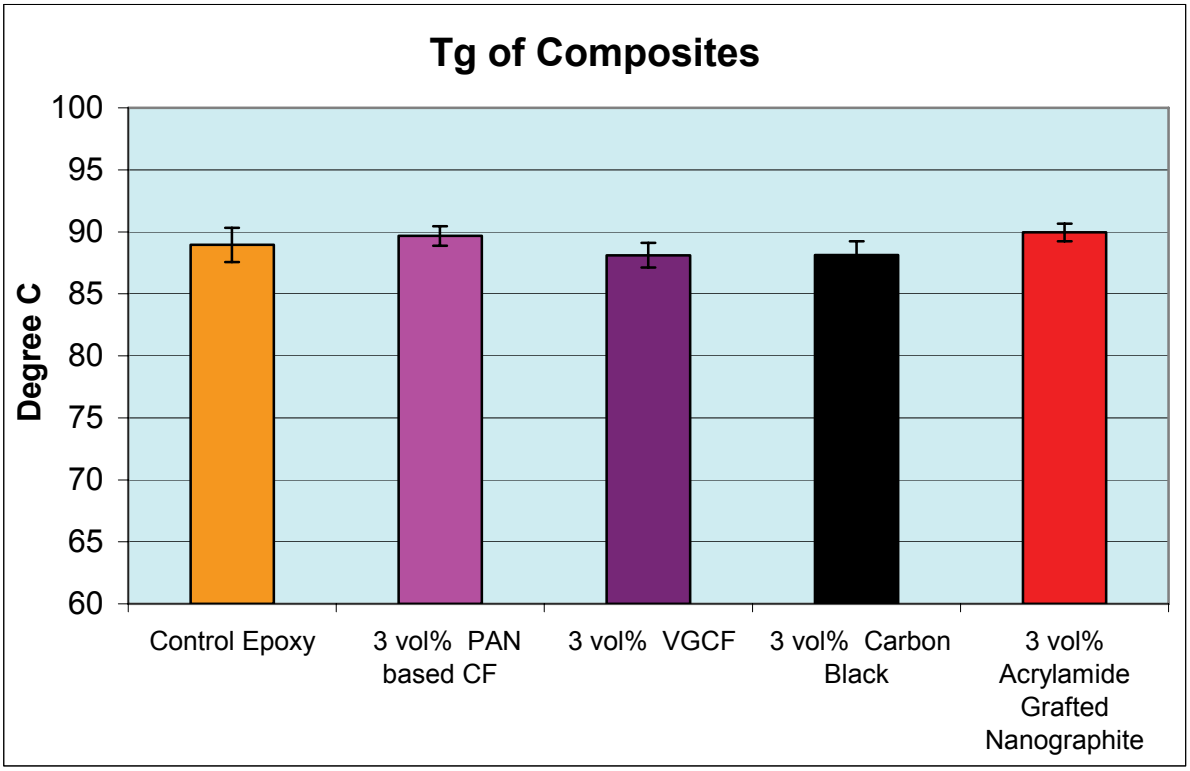

Figure 32. Tg of Composite Samples filled with Carbon Materials

The Effect of Surface Treatments on coefficient of thermal expansion (CTE).
Composites were fabricated reinforced with 3 vol% of nanographite platelets having O_2 plasma,

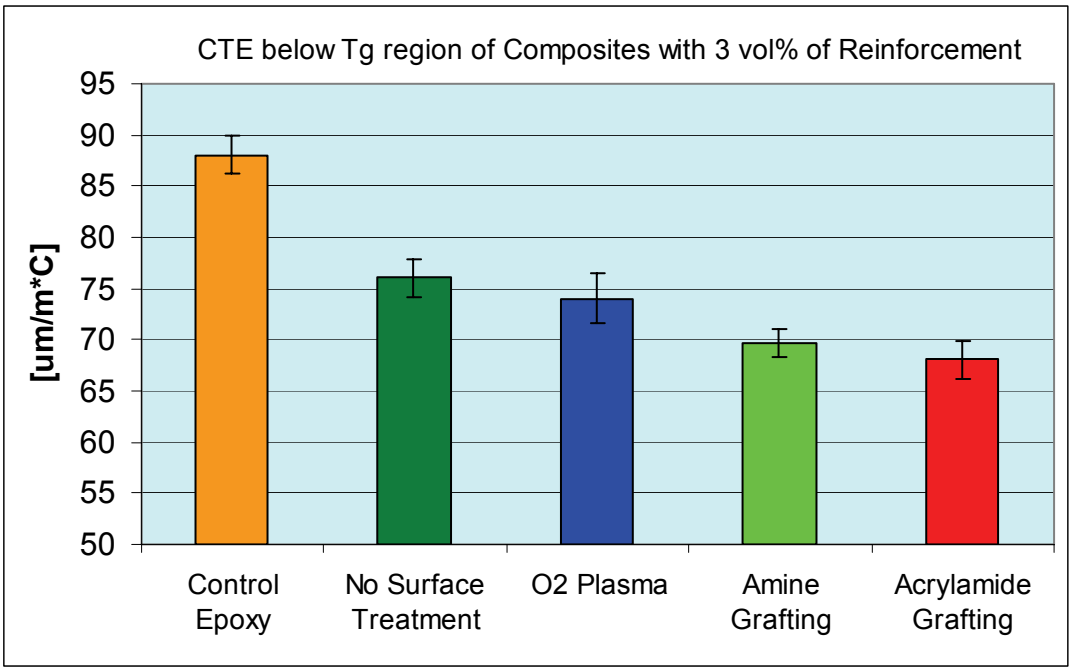

Figure 33. CTE (below Tg) of Composite Samples filled with Nanographite with different Surface Treatments

amine grafting, or acrylamide grafting treatments. Control epoxy samples were also made. CTE of these samples were measured using Thermomechanical Analysis (TMA) and the data are summarized in **Figures 33** and **34**.

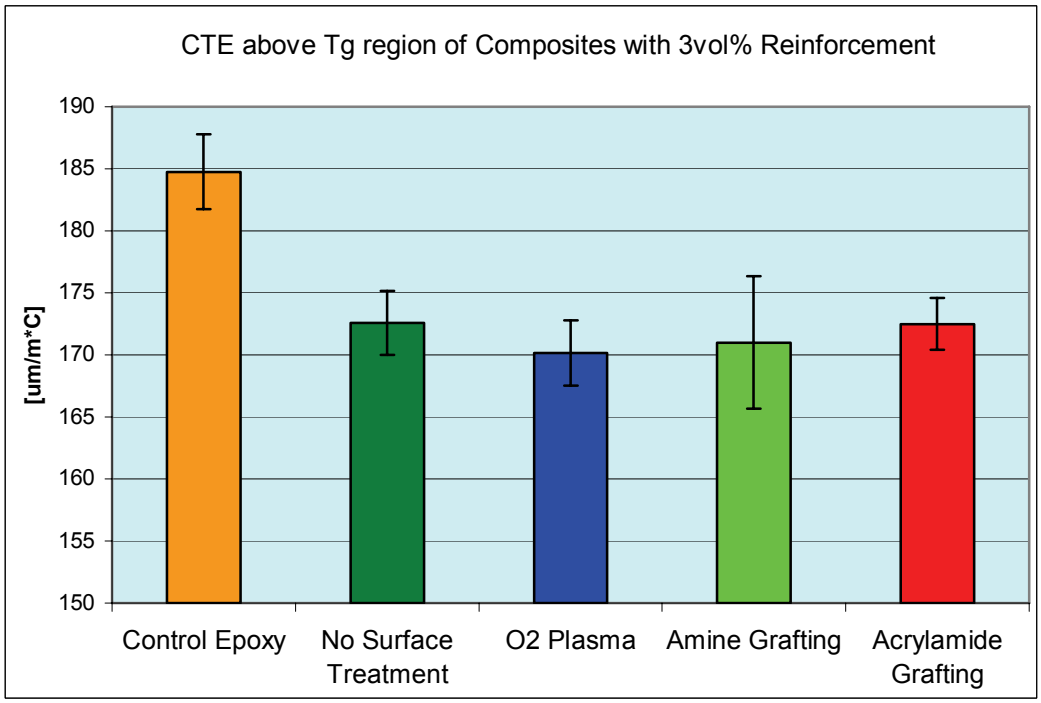

Figure 34. CTE of (above Tg) Composite Samples filled with Nanographite with different Surface Treatments

Below Tg, nanographite with surface treatments showed lower CTEs, (better dimensional stability). Nanographite treated with the acrylamide grafting showed about 23% lower value than the control epoxy. Surface treatments did not affect the CTE above Tg, but each composite sample showed about a 7% improvement compared to the untreated graphite.

Below Tg, nanographite treated with acrylamide grafting showed the lowest CTE. Thus, it is concluded that acrylamide grafted nanographite sample had better interactions with the matrix and was considered to be a better reinforcement compared to the commercially available carbon materials used in this research.

Summary. Newly developed graphite nanoplatelets were used as reinforcements in an epoxy matrix. It was revealed that the size of the platelets affected the properties of composites, since smaller platelets had larger edge area and more functional groups. Several surface treatments were investigated to improve the surface condition of the graphite and acrylamide grafting was found to be very effective to enhance the interaction between the graphite sample and the epoxy matrix. The composites reinforced with acrylamide-treated graphite nanoplatelets showed better mechanical properties than those reinforced with commercially available carbon materials.

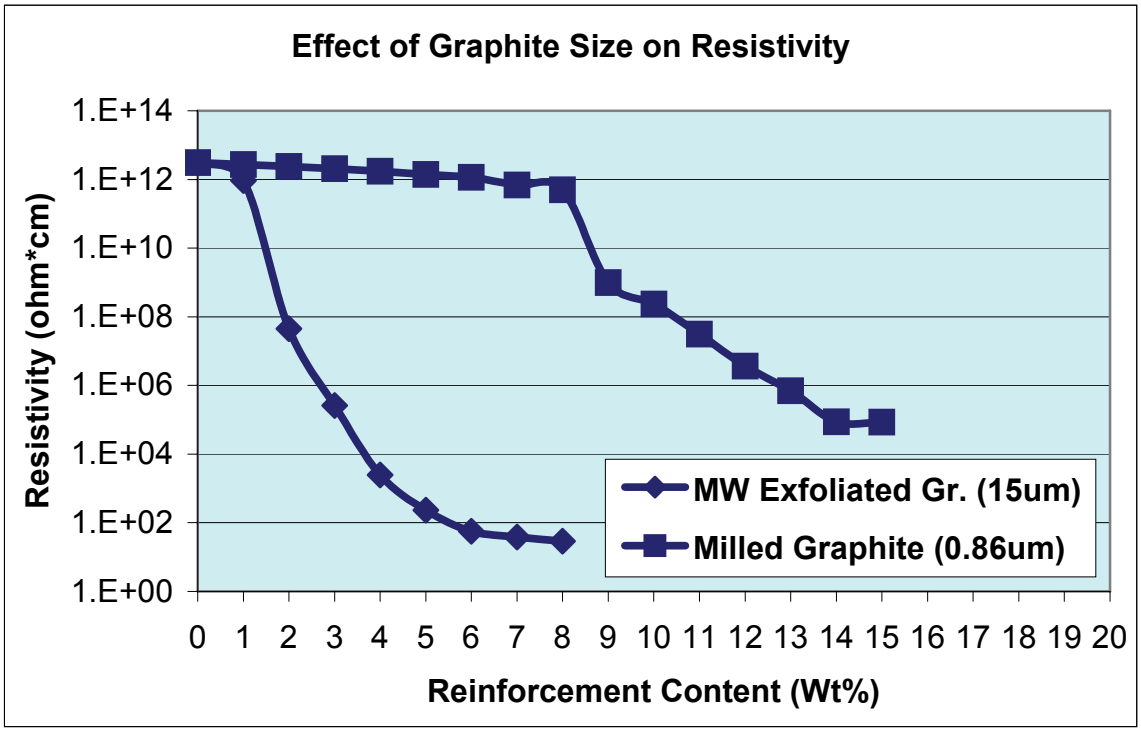

Figure 35. Resistivity of Composite Samples filled with Different Size Exfoliated Graphite Samples

ELECTRICAL PROPERTIES

Effect of Graphite Platelet Size. **Figure 35** shows the resistivity data of composites filled with graphite platelets of different sizes. They reveal that the percolation threshold of composites

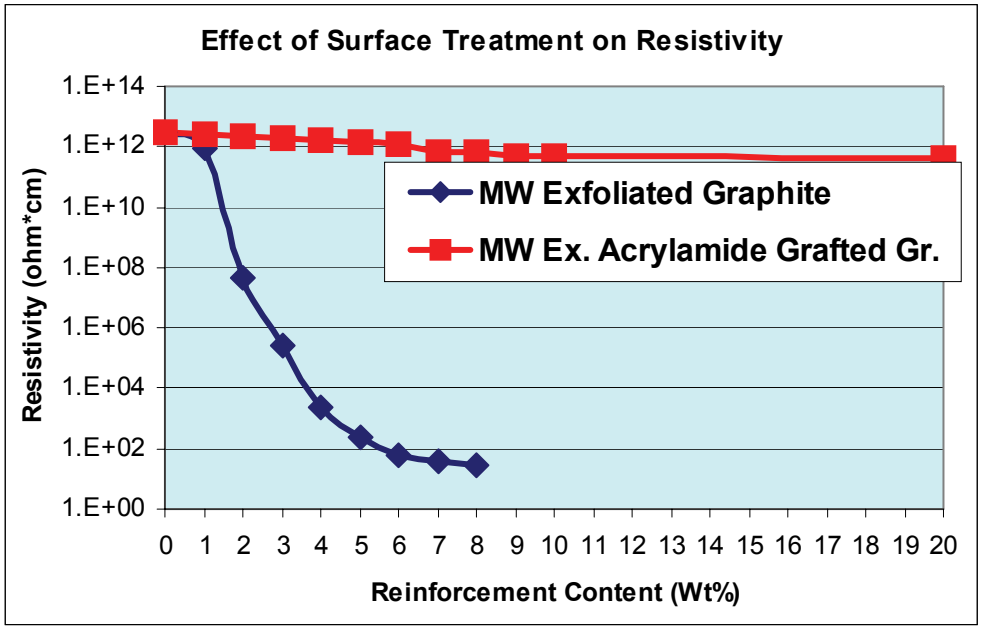

Figure 36. Resistivity of Composite Samples filled with Graphite with Different Surface Conditions

filled with larger graphite platelets is much smaller than that of composites with smaller platelets. Fillers with higher aspect ratios can make a conducting path at a lower filler content in a composite system, which leads lower percolation threshold. Because the larger graphite platelets have much larger aspect ratio (about 1500) than the smaller graphite platelets (aspect ratio = 78), it is reasonable that the larger graphite platelets showed a lower percolation threshold.

Effect of Surface Treatment Condition of Graphite Platelets. **Figure 36** shows the resistivity of composites filled with graphite platelets with or without acrylamide grafting treatment. The percolation threshold of composites filled with graphite platelets with no surface treatment was much smaller than that of composites with acrylamide grafted platelets. It is known that the dispersion condition of fillers in the matrix affect the percolation data significantly. The acrylamide grafting treatment has proved to be a very good surface treatment for improving the mechanical properties. However, the amount of acrylamide grafted onto the platelets may have also acted to coat the platelet edges with polyacrylamide and could also act to insulate the edges and prevent good electrical contact. In such a condition, it is difficult to make a conductive path through out the composite system.

Comparison of Various Carbon Materials. **Figure 37** shows the resistivities of composites filled with various carbon materials. Composites filled with exfoliated graphite platelets showed the same percolation threshold and resistivity as composites filled with carbon black or VGCF.

Percolation Theories. According to percolation theory, the effective resistivity can be written as;

$$\rho_{eff} = \rho_0 (p - p_c)^{-t} \qquad \text{for } p > p_c \qquad (1)$$

where ρ_{eff} is the effective resistivity of the composite, ρ_0 is the resistivity of the conductive phase, p is the volume fraction of the conductive phase, p_c is the percolation threshold, and t is the conductivity exponent. Equation (1) can be rewritten as

$$\log\left[\frac{\rho_{eff}}{\rho_0}\right] = -t \bullet \log[p - p_c] \qquad \text{for } p > p_c \qquad (2)$$

Thus, t can be determined by a least-square linear fit of log $[\rho_{eff}/\rho_0]$ vs log $[p-p_c]$ data. The parameters p_c, t, and ρ_0 coupled with this analysis is called the three-parameter fit analysis. Gaines et al. showed that a change of p_c by 0.5% changed t by 0.5, which could lead to inaccurate data analysis [28,29]. Therefore, they recommended determining p_c experimentally to eliminate the ambiguity of the conventional three-parameter fit method.

In the following analysis, the preliminary percolation threshold value was first determined from the experimentally obtained resistivity data. Then, the least-square linear fit of log $[\rho_{eff}/\rho_0]$ vs log $[p-p_c]$ was performed to obtain t by changing ρ_0 and p_c. During the fitting, the change in the p_c value was limited to 0.2% to reduce inaccuracies. Once t, ρ_0 and p_c were determined, these values were substituted into equation (1) and a resistivity curve was made and compared to the experimental data.

Microwave-exfoliated Nano Graphite Platelets. **Table 8** shows the values of the percolation threshold, p_c, the resistivity of conductive phase, ρ, and the conductivity exponent, t. **Figure 38** shows the prediction and experimentally obtained resistivity curves using the value of 3.12 fot t.

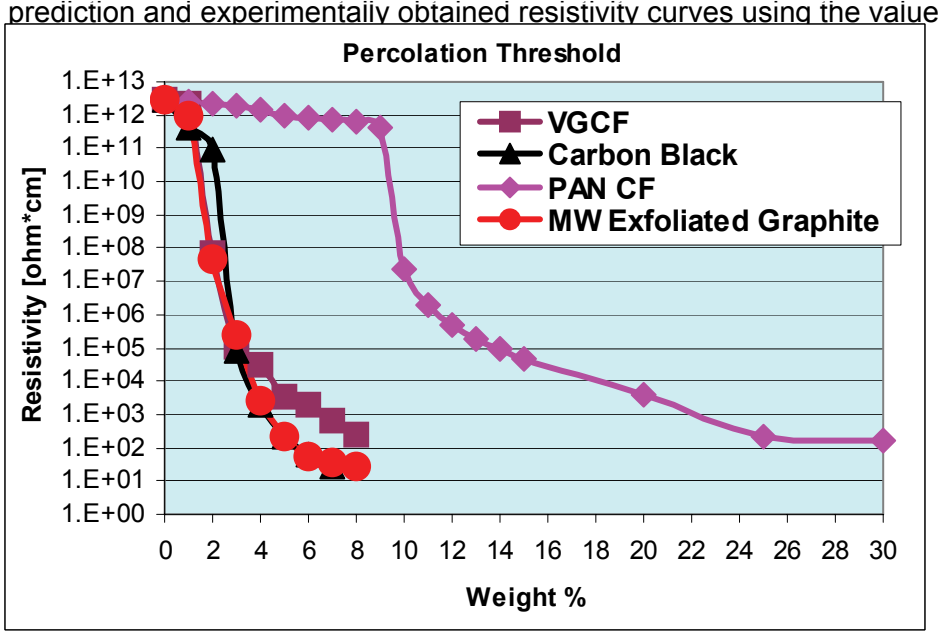

Figure 37. Experimentally obtained Resistivity for Microwave Exfoliated Graphite System and Other Carbon Materials

Table 8. Results of Percolation Analysis for Microwave Exfoliated Graphite System				
Reinforcement	p_c (Vol%)	p_c (Wt%)	ρ ohm*cm	t
MW Exfoliated Gr.	1.13	1.93	0.001	3.12

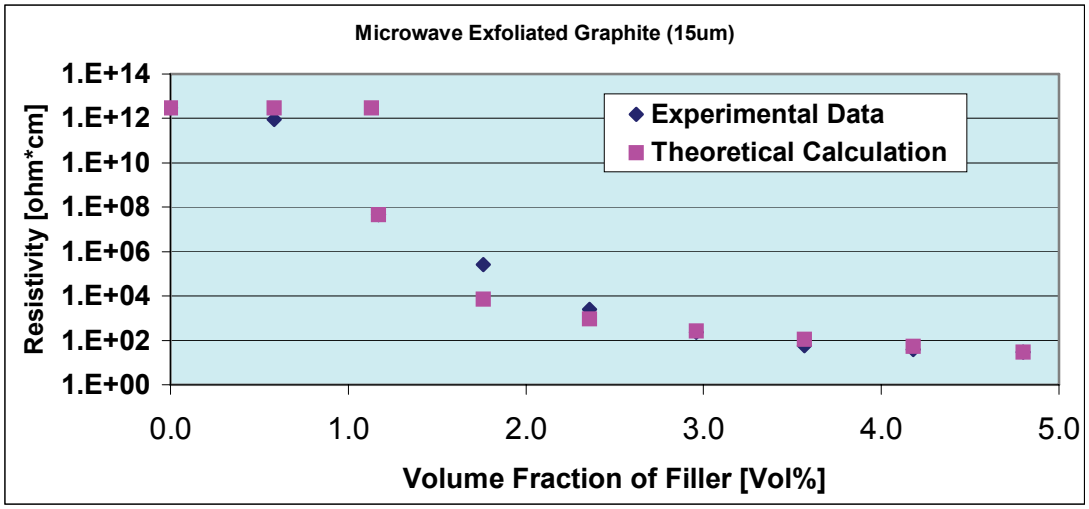

Figure 38. Theoretical and Experimentally obtained Resistivity for Microwave Exfoliated Graphite System

Table 9. summarizes the values of the percolation threshold, p_c, the resistivity of conductive phase, ρ, and the conductivity exponent, t for all carbon materials investigated.

Table 9. Results of Percolation Analysis for Various Carbon Material based Composites

Reinforcement	p_c (Vol%)	p_c (Wt%)	ρ ohm*cm	t
MW Exfoliated Gr.	1.13	1.93	0.001	3.12
MW and Milled Gr.	4.90	8.17	15	3.24
CF	5.90	9.76	0.4	3.26
VGCF	1.09	1.87	0.03	3.03
Carbon Black	1.29	2.00	0.01	3.03

The analysis of the experimental data gave values for the conductivity exponent of about 3. and shows that the microwave-exfoliated graphite platelets could percolate around 1.1 vol% (1.9 wt%), which is comparable to the data for commercially available VGCF and carbon black samples.

THERMAL CONDUCTIVITY

Thermal conductivity of composites filled with microwave-exfoliated graphite platelets was measured indirectly by using DSC with gallium as the standard. Thermal conductivity was measured using DSC. A quartz standard 6 mm in diameter and 3.49 mm thick was placed in an open DSC pan. A 41.0 mg sample of gallium was placed on top of the disk. The DSC cell was ramped 2ºC/min to 40ºC to melt the gallium and provide intimate contact with the quartz. Temperature was ramped 2ºC/min to 20ºC. Heat flow and temperature data was then collected while ramping the temperature at 2ºC/min to 40ºC. This same procedure was used for each 6 mm diameter rubber disk. The same gallium sample was used for all measurements. Rubber samples were punched from each of the 0 phr carbon black sheets using an arch punch and press. The thickness of each rubber disk was measured. The Heat Flow/Temperature slope (m) through the melt was calculated for the quartz and rubber samples. Thermal conductivity (K) was calculated as:

$$K_r = (m_r^2 / m_q^2) \times T_r/T_q \times K_q$$

Where:

K_r = Thermal conductivity of rubber sample

K_q = Thermal conductivity of quartz standard = 1.37 W/mºK (literature value)

m_r = Slope of Heat Flow/Temperature through melt- Ga on rubber

m_q = Slope of Heat Flow/Temperature through melt- Ga on quartz = -0.08899 W/g/ºC

T_r = Thickness of rubber sample

T_q = Thickness of quartz standard = 3.49 mm

Figure 39 shows the results on a logarithmic scale. (Electrical conductivity data are included for comparison.) The trends in both the electrical and thermal conductivity are very similar except that the electrical conductivity changes by 10 orders of magnitude while the thermal conductivity changes by just 1 order.

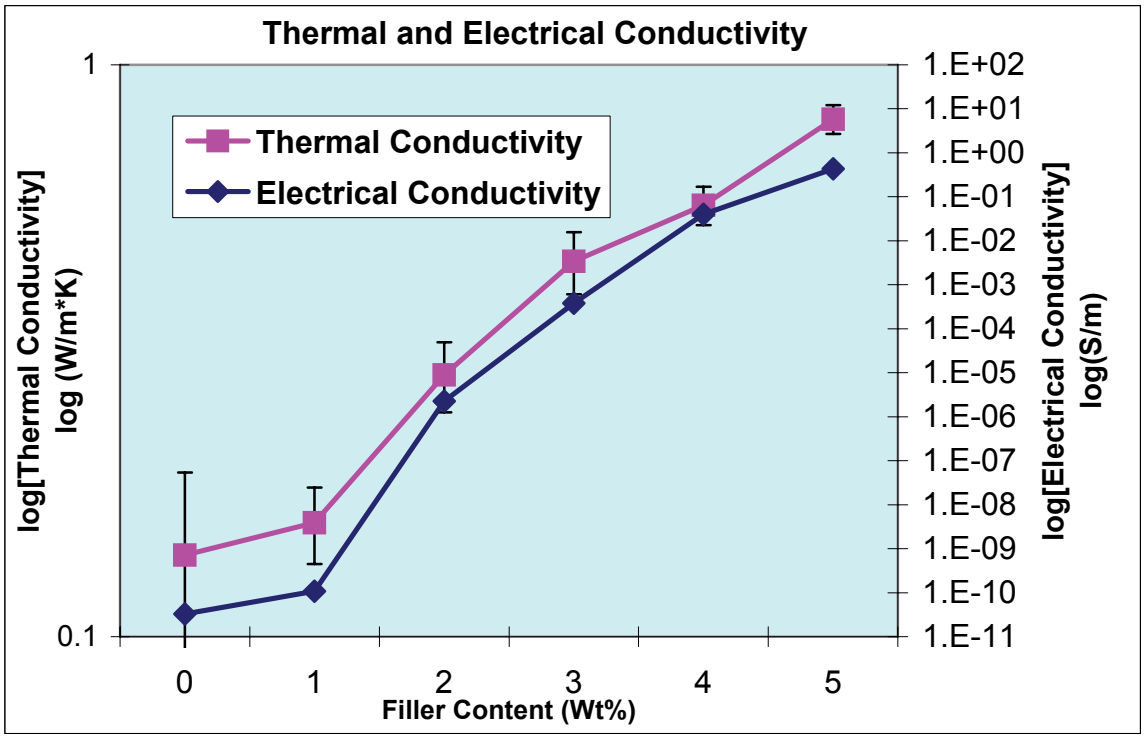

Figure 39. Thermal and Electrical Conductivity of Composites filled with Microwave-exfoliated Graphite Platelets

Figure 40 compares the thermal conductivities of composites filled with various carbon materials. Composites filled with exfoliated graphite showed the highest thermal conductivity. The platelet morphology of the exfoliated nanographite is suspected to be responsible for the disparity in results. The platelets can overlap with a relatively large contact area while the cylindrical and spherical shaped particles can only exhibit point contact resulting in high thermal contact resistance.

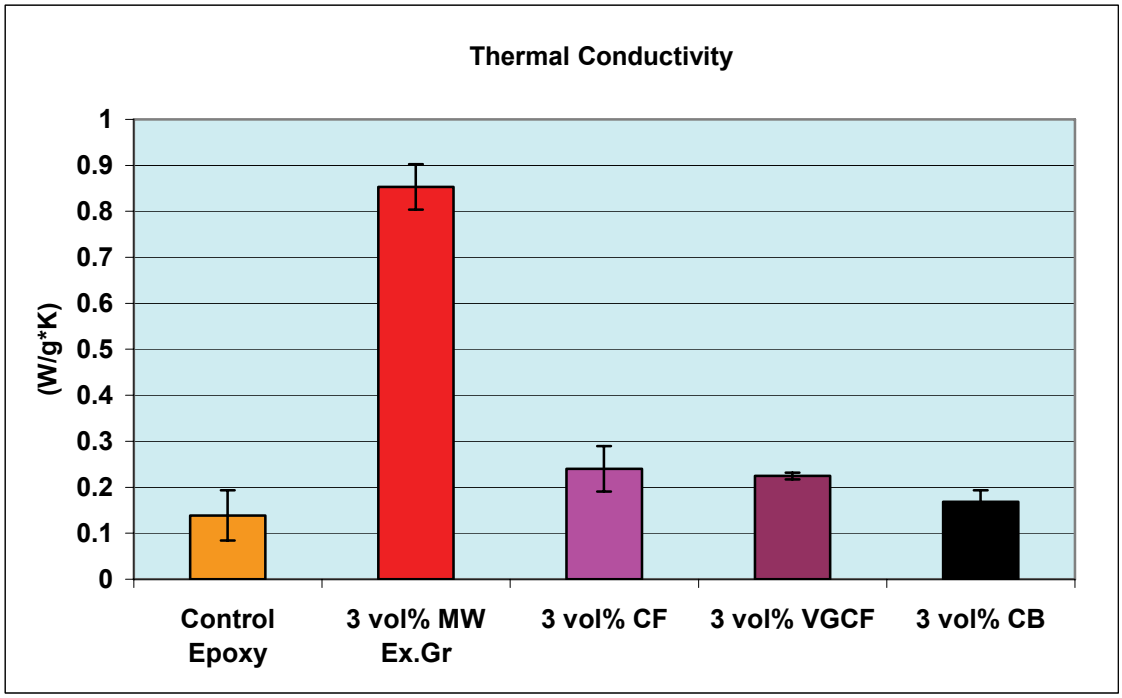

Figure 40. Thermal Conductivity of Composites filled with Various Carbon Materials

DIELECTRIC PROPERTIES

Dielectric properties of composite samples were calculated from Impedance Spectroscopy data. The measurement gives the real and imaginary parts of impedance, Z' and Z", over a frequency range of 0.1 to 100,000Hz.

Figure 41 shows the dielectric constant and loss factor of composite samples filled with various carbon materials. The dielectric constant at low frequency is a measure of the concentration of permanent polar functional groups. When compared at the same concentrations, these results imply that the microwave-exfoliated graphite and carbon black have the highest density of polar groups. The XPS data showed that the carbon fiber sample had the highest oxygen and nitrogen content but the surface area of the carbon fiber is about a factor of 200 less than the graphite platelets and the carbon black particles.

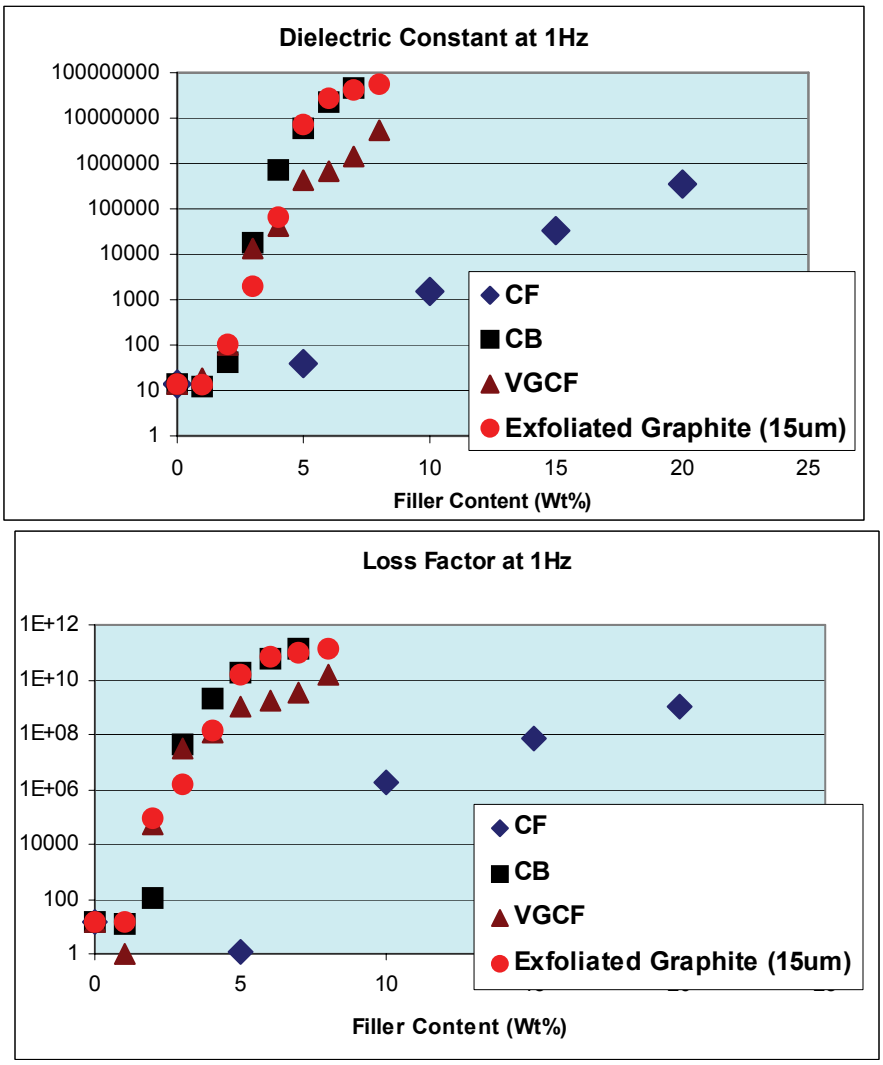

Figure 41. Dielectric Constant and Loss Factor at 1 Hertz of Composites filled with Various Carbon Materials

SUMMARY

The electrical conductivity of graphite nanocomposites was investigated. The results revealed that the exfoliated graphite sample with a high aspect ratio was an excellent conductive filler, showing a comparable or better percolation threshold and conductivity to conventional fillers. Thermal conductivity data also proved that this new graphite material was the best filler among the carbon materials investigated. From these results and the predicted low cost ($ 5/lb), this new type of graphite material developed at MSU has a realistic possibility of replacing conventional carbon materials or newly developed nanomaterials. The possible application fields are broad, including automobile, electrical/electronics, aerospace, and military industries.

STRESS ANALYSIS IN PARTICULATE COMPOSITES

Background

Failure mechanisms of materials can be classified into several categories such as the yielding of ductile materials, the fracture of brittle materials, fatigue, and buckling. In the case of short-fiber reinforced polymer composites, the fracture process could be a combination of multiple mechanisms. If the bonding between matrix and fibers was perfect, the failure would occur by either the plastic deformation of the matrix or the breakage of a fiber. In practice, however, most composite failures are initiated by interfacial debonding around reinforcements. SEM observations of the failure process of a short-fiber reinforced composite revealed that the process included several sequential steps [30,31].

- Interfacial debonding at the fiber ends
- Plastic deformation of matrix around the fibers
- Interfacial microcrack propagation along fiber sides
- Catastrophic crack propagation throughout the matrix

Thus, it is important to investigate the adhesion condition between fibers and matrix and stress concentrations at the interface and in the nearby matrix to predict failure.

The adhesion condition between fibers and a polymer matrix can be investigated experimentally by testing methods such as the fiber pullout test, the microdrop technique, and the single fiber fragmentation test [32],but it is difficult to assess the interfacial bond quality of flake-reinforced composites because of the inconsistency of the dimensions of the platelets. However, the stress distribution in the interface region of these composites can be simulated by using the finite element method.

To describe plastic deformation phenomena, the von Mises yield criterion [33] is most widely used because it can provide agreement between theory and experimental results in many cases. This model assumes that the failure of a ductile material occurs when the energy of distortion reaches the yield energy of the material. The criterion is mathematically expressed as

$$\sigma_{yield} \geq \sigma_{eff} = \frac{1}{\sqrt{2}}\left[(\sigma_1 - \sigma_2)^2 + (\sigma_2 - \sigma_3)^2 + (\sigma_3 - \sigma_1)^2\right]^{1/2} \quad (1)$$

where σ_{eff} is the effective stress of the material and σ_1, σ_2 and σ_3 are the stresses in directions 1, 2, and 3. In the case of plane stress, only σ_1, σ_2 and σ_3 exist. So the equation becomes,

$$\sigma_{yield} \geq \sigma_{eff} = \left(\sigma_1^{\,2} - \sigma_1\sigma_2 + \sigma_2^{\,2}\right)^{1/2} \quad (2)$$

The von Mises stress of composite systems can also be simulated by using the finite element method.

An inclusion in a polymer matrix usually causes a stress concentration, which could initiate cracking and/or plastic failure. The stress field can be affected by many factors such as the shape the inclusion, the morphology of the system, a mismatch in expansion/shrinkage, and the adhesion between matrix and inclusions. To design good composite systems for a specific application, it is important to understand the effects of these factors on the properties of composite systems.

To evaluate the local stress fields of composite systems, single inclusion models were investigated first [34,35]. These models represent the dilute inclusion condition. When inclusions are closely packed, on the other hand, the stress fields from the inclusions interact with each other, forming very complex stress fields. To solve this problem, a new concept called the

effective medium approach has been introduced [36,37,38]. In this case, theoretical calculations usually assume that the inclusions are arranged in periodic ways [39,40,41,42,43]. This approach is useful to predict the effective (global) elastic and thermal constants, but it cannot handle the local stress fields in composite systems with randomly oriented inclusions.

In real composite systems, the dispersion of inclusions is generally disordered. To investigate the effect of the arrangement of inclusions on the local stress fields and effective properties, models with two neighboring inclusions have been used [44,45,46].

The objective of this research was to investigate the effect of the shape and geometric arrangement of inclusions on the local stresses in nanocomposite systems. . The factors investigated were (1) the shape of an inclusion, (2) the aspect ratio of an inclusion, and (3) the geometric arrangement of inclusions. Single-inclusion finite element models were used to investigate the first two factors while two-inclusion models were used to investigate the last one. In the case of two-inclusion models, the inclusions were not allowed to overlap each other. To focus on these factors, perfect bonding between inclusions and matrix was assumed and no residual stress due to the difference in CTE (coefficient of thermal expansion) between matrix and inclusion was considered.

Finite Element Method

The software used was ANSYS 57. In the simulation, the quadrilateral plane elements were used so that each element was defined by eight nodes and each node had two degrees of freedom in the x- and y- directions. All the simulations were done under the plane stress condition. By assigning symmetric boundary conditions on the x- and y- axis, only a quarter of the whole model system was required to be input as a simulation model. The engineering constants of the matrix and graphite material are summarized in **Table 10**. [47]

Table 10. Engineering Constants of Matrix and Graphite Sample

	Matrix	Inclusion
	Epoxy	Graphite
	Isotropic	Transversely Isotropic
Young's Modulus ($E_{11} = E_{22}$)	2.5 MPa	1,060 MPa
Young's Modulus (E_{33})		36.5 MPa
Poisson's ratio ($\nu_{12}\nu_{21}$)	0.35	0.165
Poisson's Ratio ($\nu_{13}\nu_{23}$)		0.343
Shear Modulus ($G_{12} = G_{21}$)		440 MPa
Shear Modulus ($G_{13} = G_{23}$)		4.5 MPa

Description of Finite Element Models

Edge Angle

Four models were used to investigate the effect of the inclusion's edge angle against the input stress. Each model had a rhombus-shaped inclusion with different edge angles relative to the remote input stress. In this and following models, the reinforcement engineering constants in directions 1 and 2 were assigned in the X- and Y- directions, and both axes were assumed as symmetric boundaries. The length of each edge line was fixed at 5. The input stress was applied in the Y-direction on a line which is located the same distance from the top corner of each rhombus inclusion. **Figure 42** shows these models.

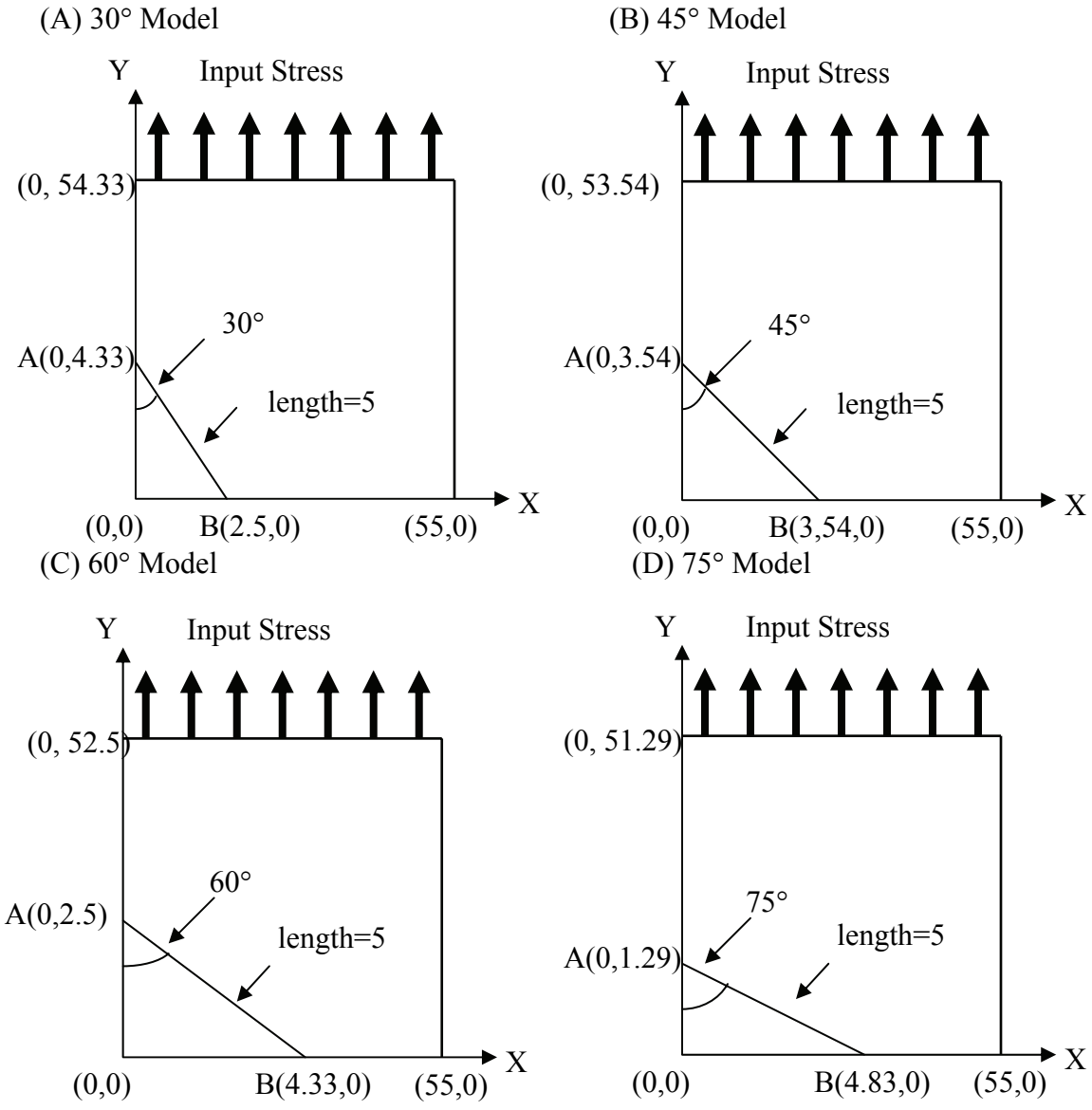

Figure 42. **The Models used to investigate the Effect of Edge Angle against Input Stress on Stress Distribution of Composite Systems**

Filler Shape

Square, circular, hexagonal, and octagonal shaped reinforcements were used as models. Two

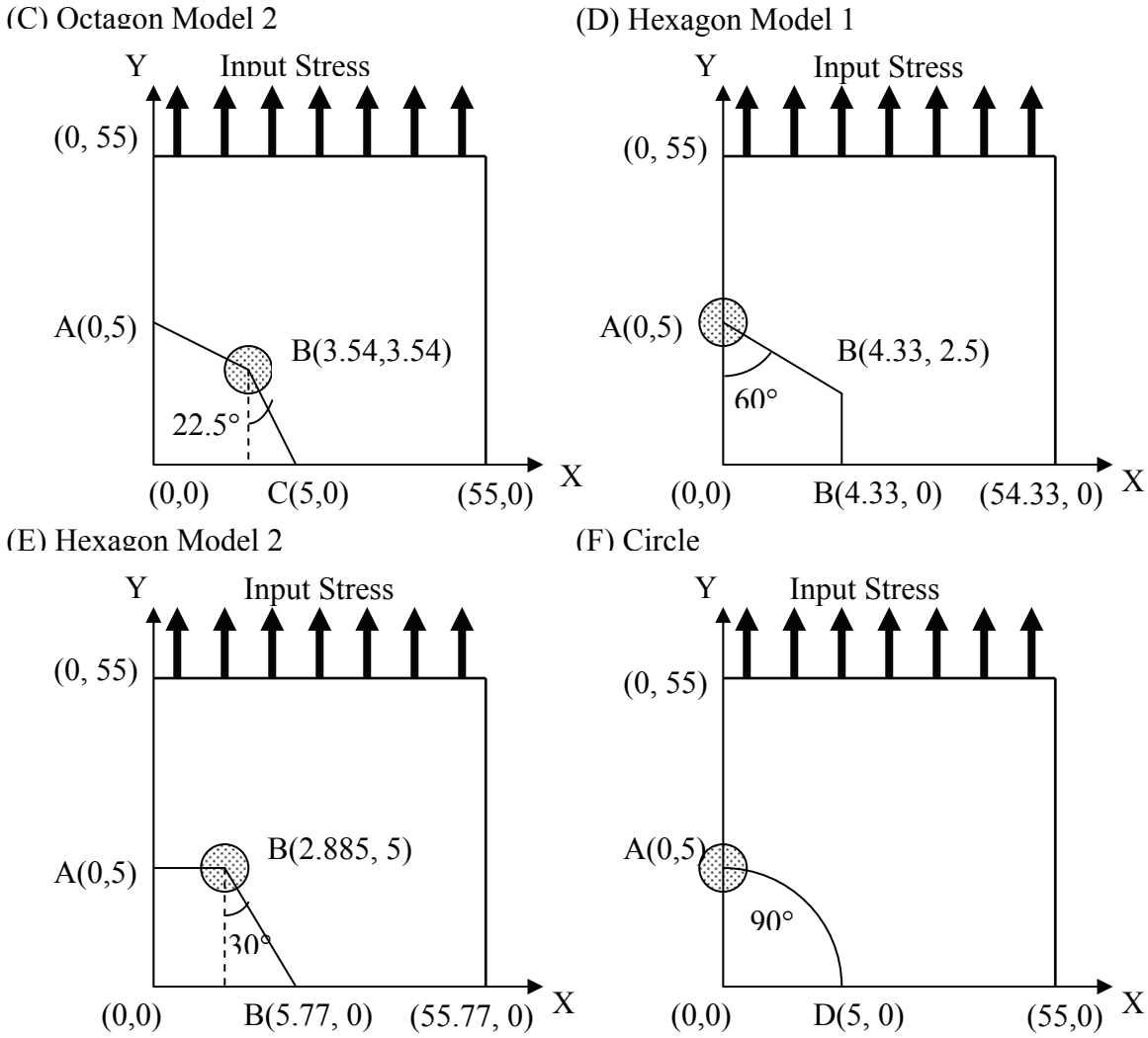

Figure 43. The Models used to investigate the Effect of Shape Difference on Stress Distribution of Composite Systems

different geometric arrangements were investigated in the hexagonal and octagonal reinforcement models. **Figure 43** shows the details of these.

Aspect Ratio

Composites with plate reinforcements with different aspect ratios were modeled. The length of the reinforcements was fixed, but the thickness was changed to adjust the aspect ratio. The aspect ratios investigated were 200, 100, 50, 20, 10, 5, and 1. The stress distribution was analyzed under two different input stress conditions, one in the X- and the other in the Y-direction. In both cases, the stresses were applied on the lines which were the same distance from the reinforcement. **Figure 44** shows the details of these models. In each model, the engineering constants of reinforcement in direction 3 were assigned as those in the X- direction and the engineering constants in direction 1 were assigned as those in the Y-direction.

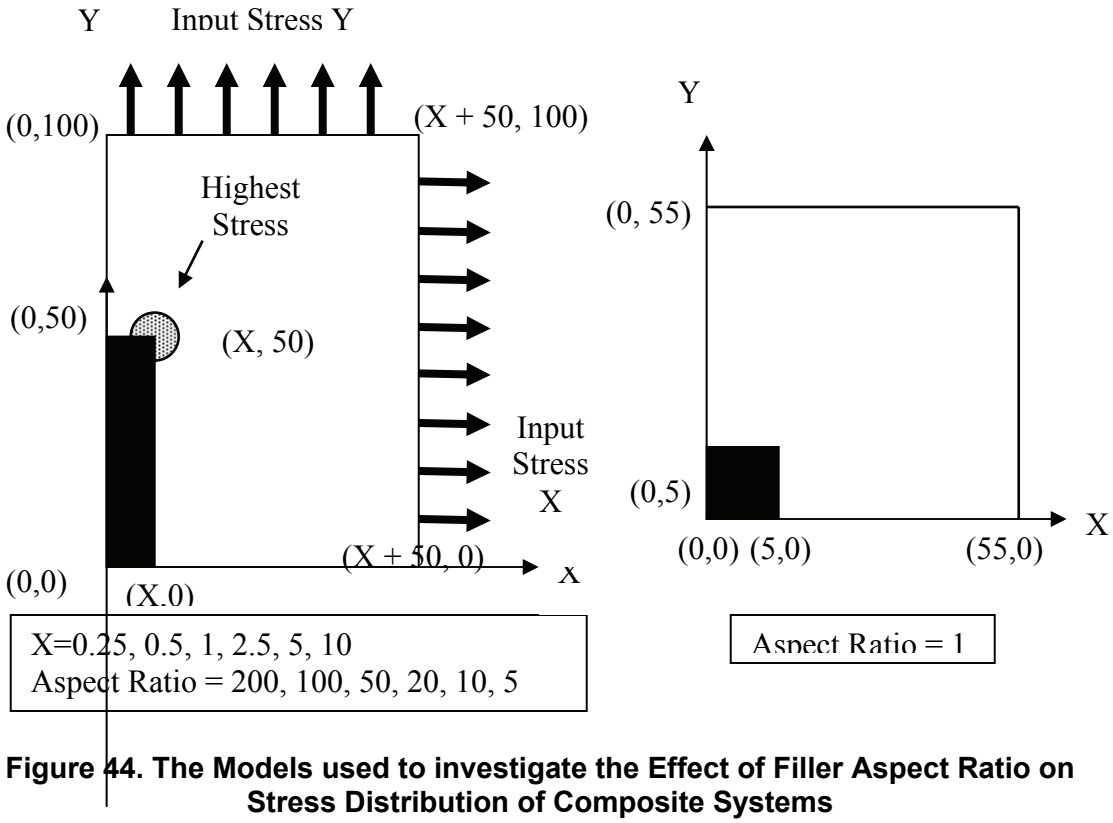

Figure 44. The Models used to investigate the Effect of Filler Aspect Ratio on Stress Distribution of Composite Systems

Distance between Aligned Fillers

Composites with two aligned plate-like filler particles with a fixed aspect ratio of 20 were modeled. The distance between the two filler particles was measured in multiples of the filler thickness. The stress distribution was analyzed under two different input stress conditions, one in the X- and the other in the Y-direction. In both cases, the stresses were applied on lines which were the same distance from the reinforcement. **Figure 45** shows the details of these models. In each model, the engineering constants of reinforcement in direction 3 were assigned as those in the X-direction and the constants in direction 1 were assigned as those in the Y-direction.

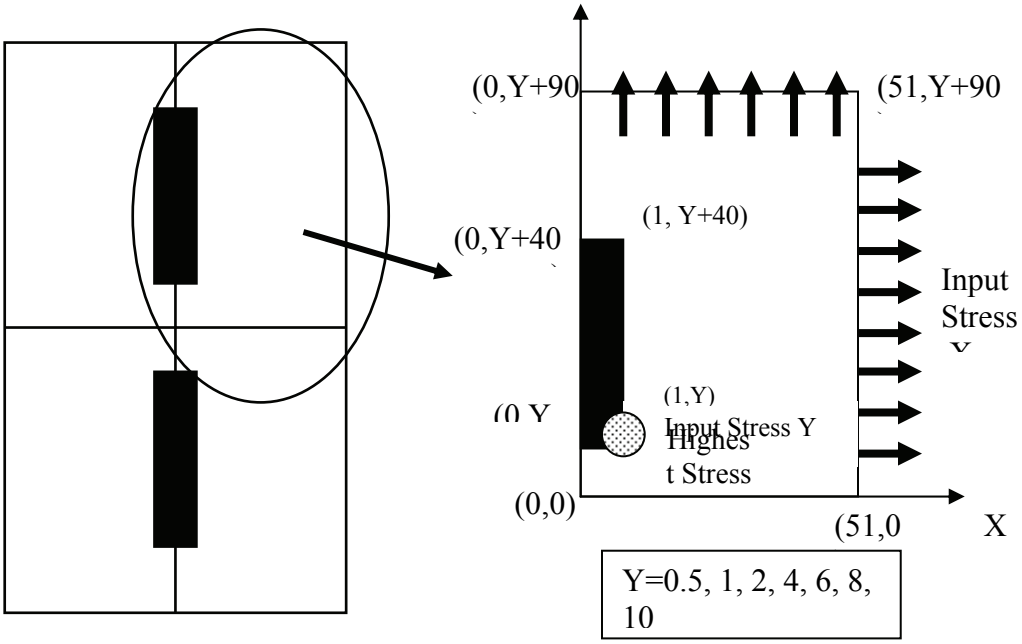

Figure 45. The Models used to investigate the Effect of Distance between aligned Fillers on Stress Distribution of Composite Systems

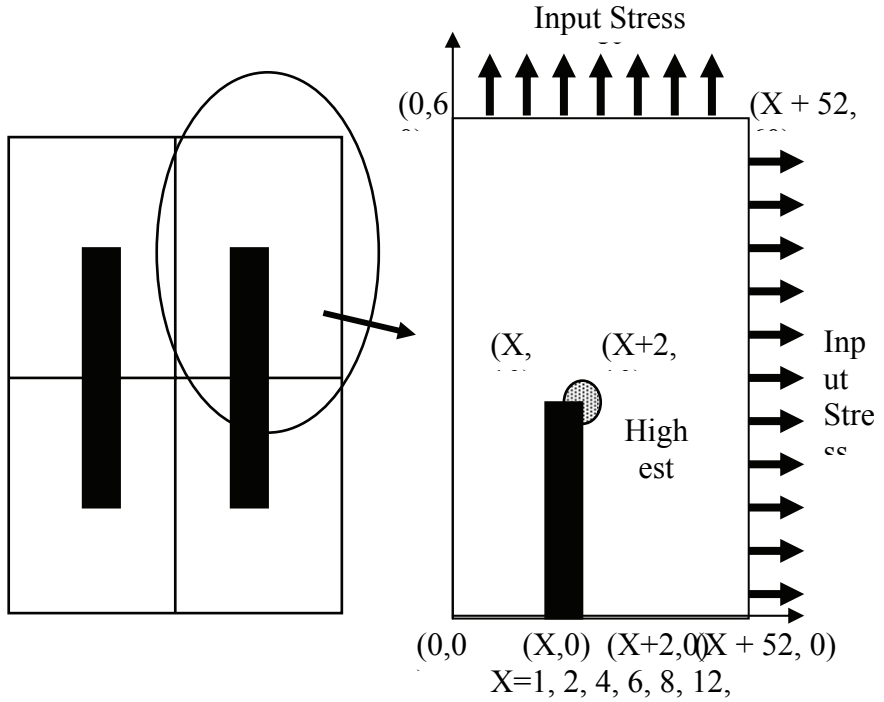

Figure 46. The Models used to investigate the Effect of Distance between Parallel Fillers on Stress Distribution of

Distance between Parallel Fillers

Composites with two parallel plate fillers with fixed aspect ratio of 20 were used as the models. The distance between two fillers was changed. The stress distribution was analyzed under two different input stress conditions, one in the X- and the other in the Y-direction. In both cases, the stresses were applied on the lines, which were the same distance from the reinforcement. **Figure 46** shows the details of these models. In each model, the engineering constants of reinforcement in direction 3 were assigned identical to those in the X-direction and the constants in direction 1 were assigned as those in the Y-direction.

FINITE ELEMENT RESULTS

Effect of The Edge Angle

The absolute values of the maximum stresses at the interface (i.e., along line 1) are summarized in **Figure 47**. The simulation revealed that the maximum stress in the Y-direction

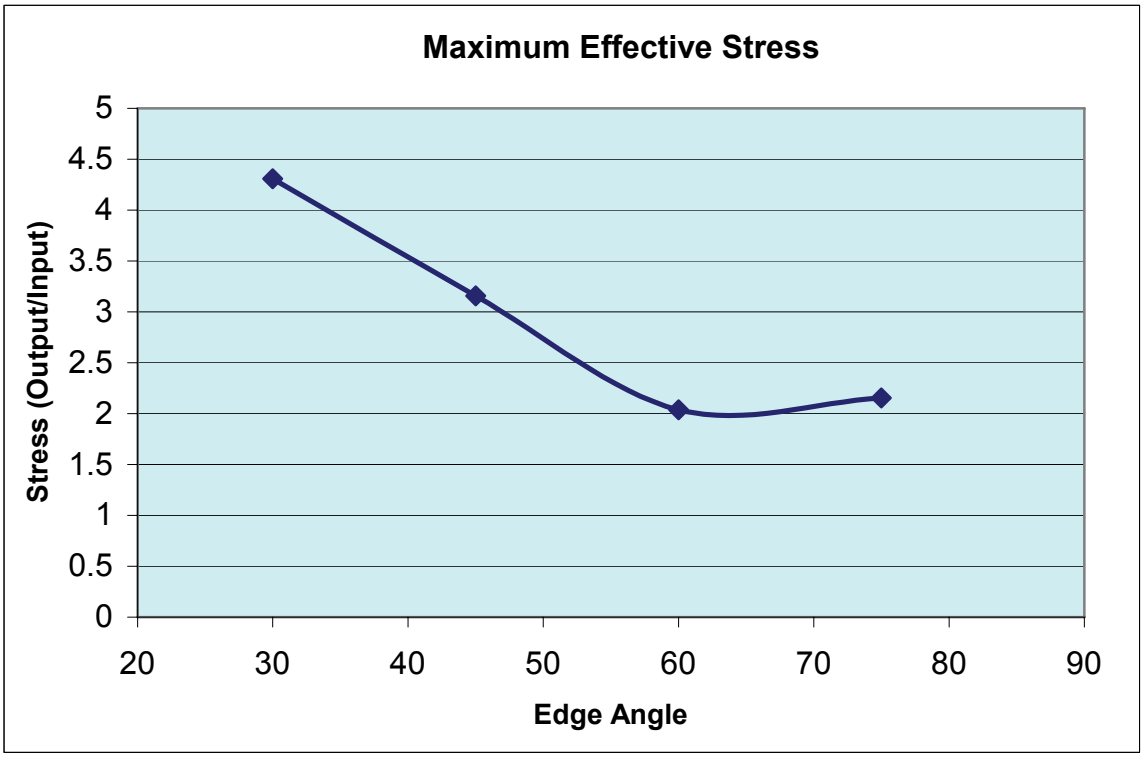

Figure 47. The effect of edge angle on the Absolute Values of Maximum stresses at the interface (on line 1)

appeared at corner A (the top corner) and was highest when the angle was the smallest. In the X-direction, the highest stress appeared at corner B (the side corner) and it was highest when the angle was the largest. The maximum shear stress appeared at either corner A or B**,** depending on the other two values, and showed a minimum as a function of angle. In all models, the stress in the Y-direction showed the highest value among these three stresses, suggesting the debonding would occur at corner A. If the adhesion condition was the same for all models, the 30° geometry would fail at the lowest input stress. In other words, this geometry produced the lowest predicted composite strength. The maximum effective (von Mises) stresses in the matrix region were calculated and the values are summarized in **Figure 48**. The simulation

revealed that the maximum effective stress decreased with increasing edge angles up to 60°, then increased a little. The maximum effective stress appeared near corner A (top corner) in the 30°-, 45°-, and 60°-models, and near corner B in the 75 ° model. Thus, if the adhesion between filler and matrix was strong enough, yielding would occur near the corners, which in turn would initiate the failure of the system. Since the 30° model shows the highest stress concentration, this model would yield at the lowest input stress. As was predicted based on the interfacial stresses, with this criterion, too, the model with a lower edge angle would show lower strength as a composite.

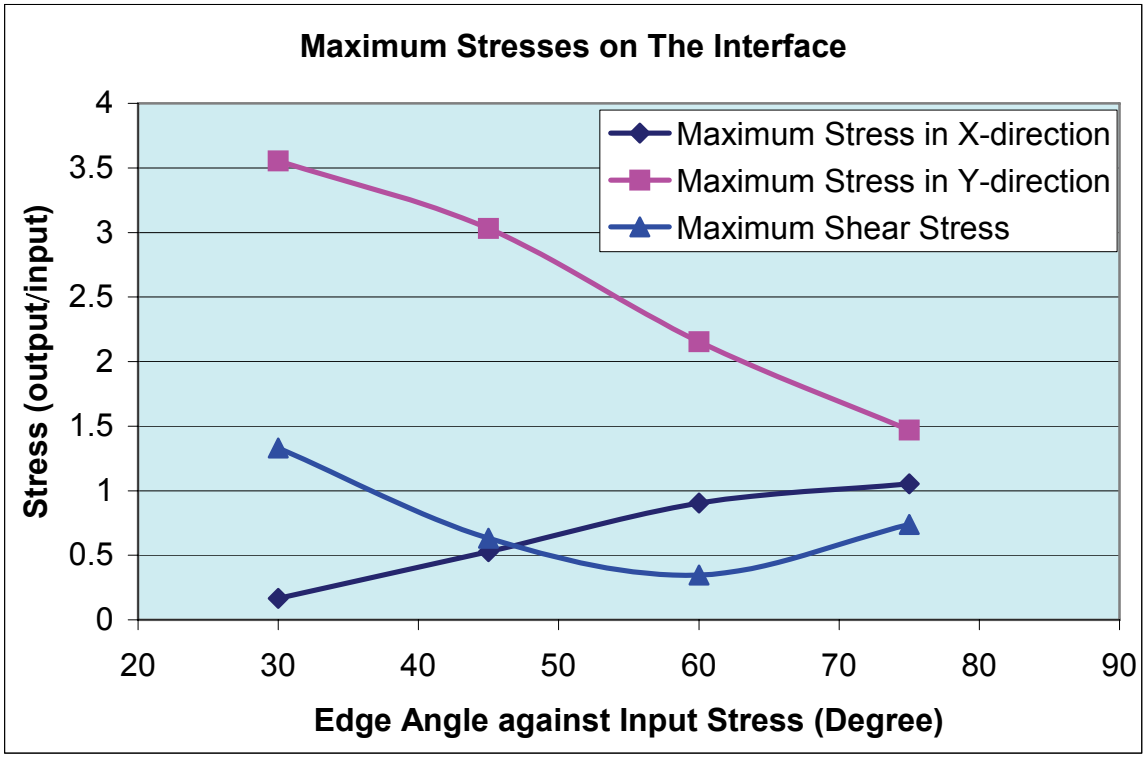

Figure 48. The effect of edge angle on the maximum effective stresses at the matrix region

Effect of Filler Shape

The absolute values of maximum stresses at the interface in each model are summarized in **Figure 49**. Hexagon Model 1 showed the highest maximum stress in the Y-direction followed by Hexagon Model 2 and Octagon Model 1, but the difference was small. Square and Octagon Model 2 had lower values, while Circle Model showed a distinctly smaller value than the others, implying this was the optimal shape to minimize stress concentration. The maximum stress in the Y-direction appeared at corner A in the case of Octagon Model 2, Hexagon Model 1, and the Circle Model, while it appeared at corner B in the other models. Since the upper edge lines of the latter models are perpendicular to the input stress, it is reasonable that the maximum stress appeared at corner B.

In the case of the stress in the X-direction, all models showed almost the same maximum stress and there was no tendency related to the filler shape. The Square model showed a higher maximum shear stress, while the Circle Model had a lower value. In this direction also, the Circle Model was the best in terms of introducing minimum stress concentration. Thus, the composite with circular shape reinforcements would stand higher input stress before it reached the point where debonding of the interface begins.

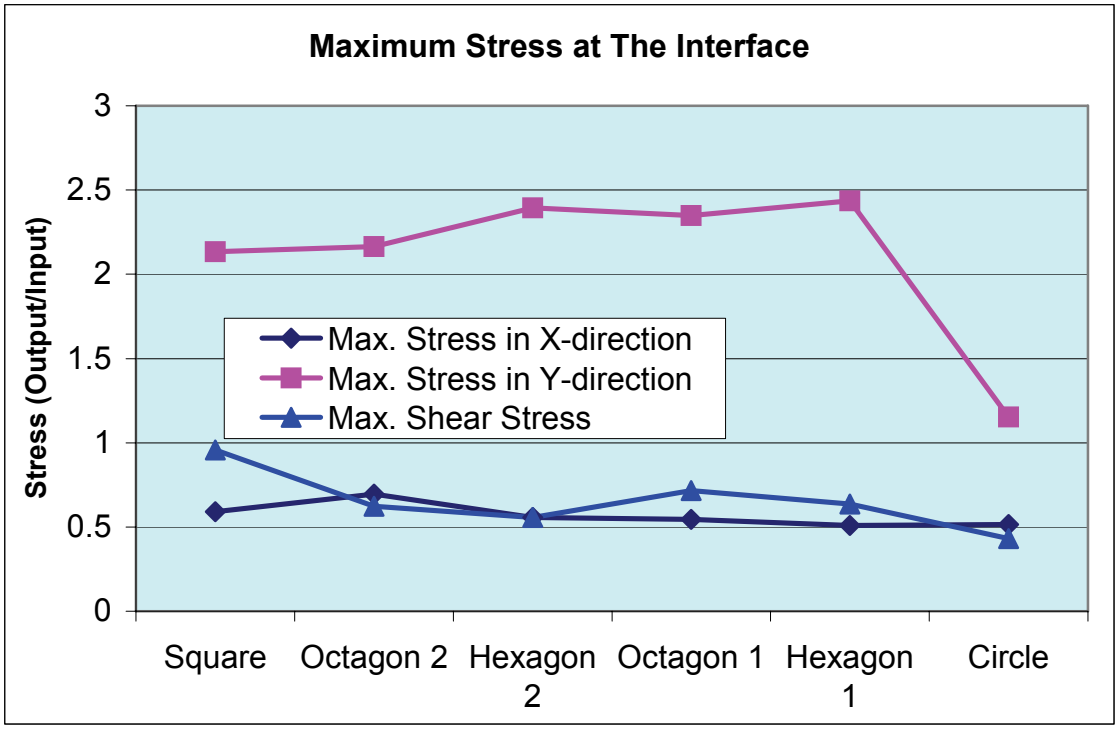

Figure 49. The effect of filler shape on the absolute values of maximum stresses at the interface

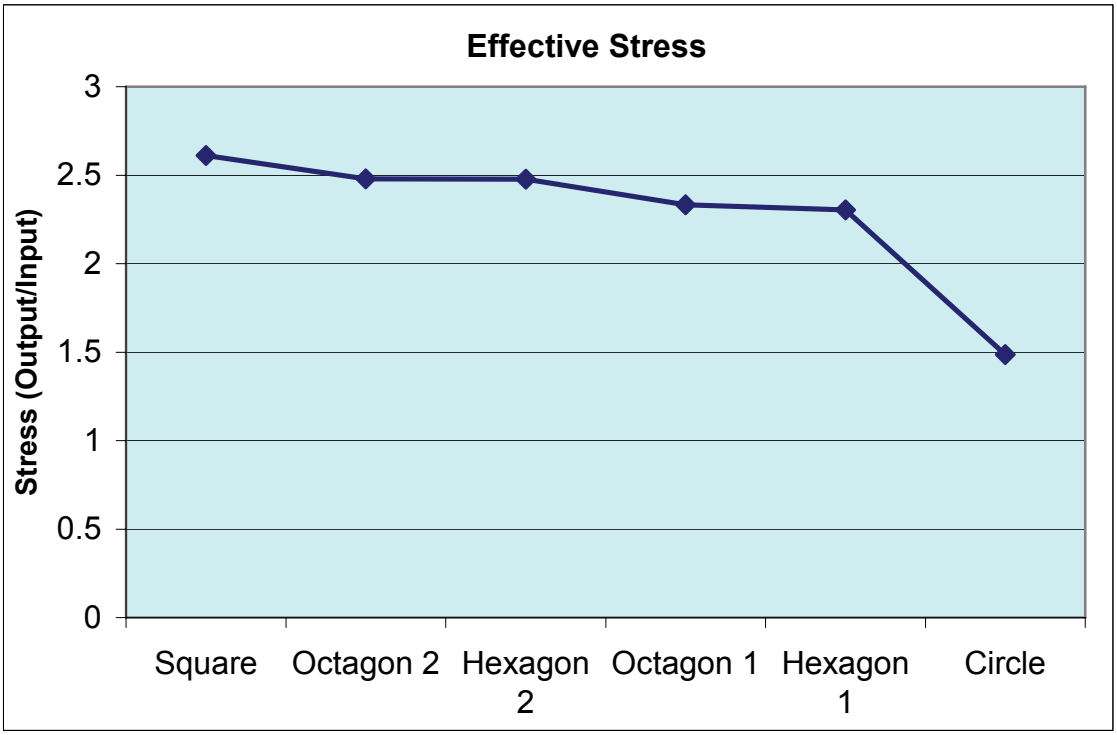

Figure 50. The effect of filler shape on the maximum effective stresses at the matrix region

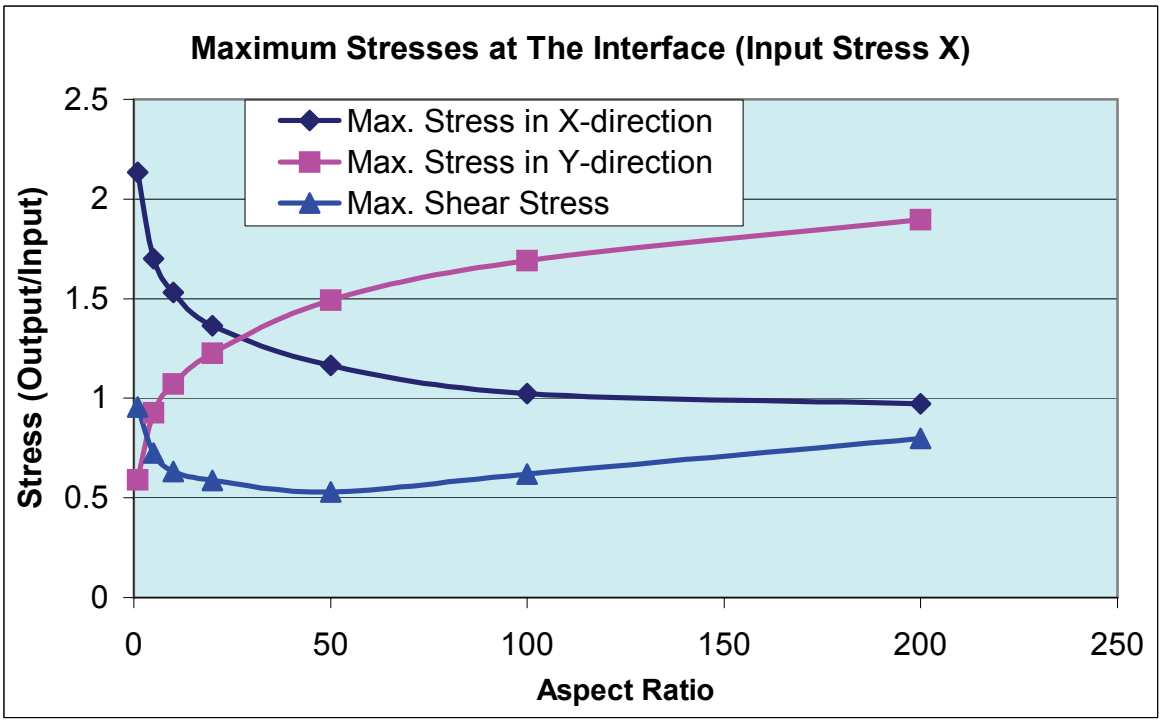

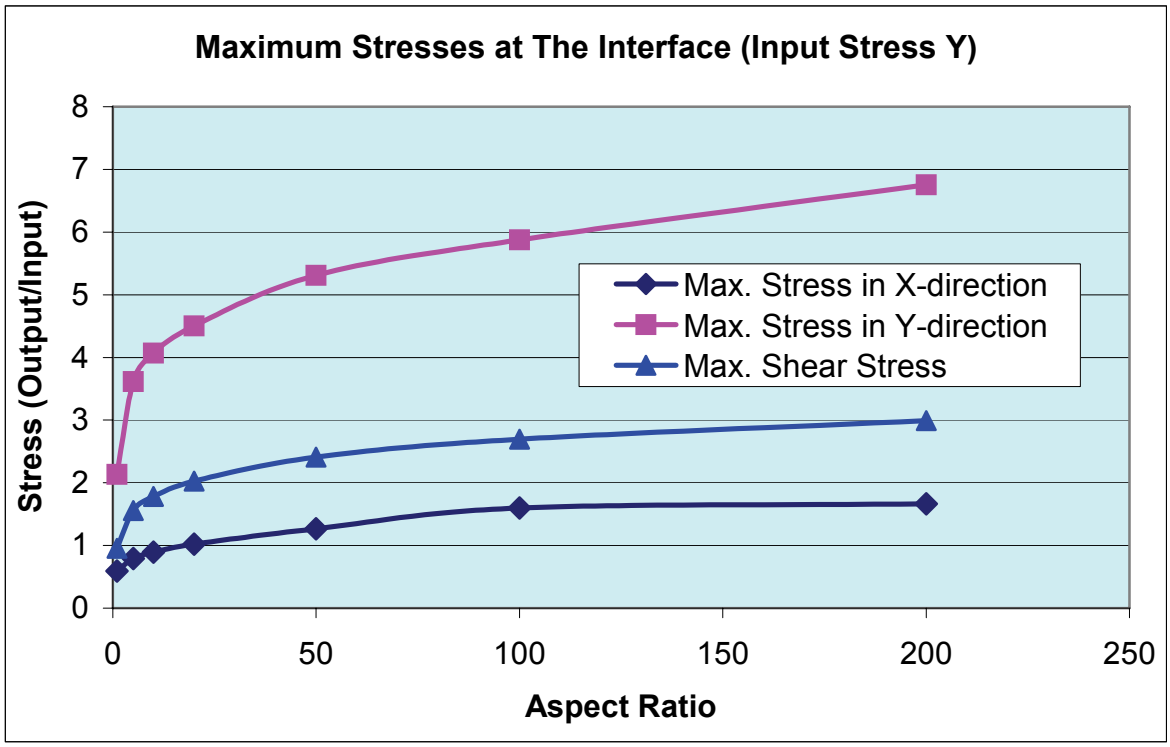

Figure 51. The effect of aspect ratio on the absolute values of maximum stresses at the interface

The maximum effective stress values in the matrix region in each model based on the von Mises equation are summarized in **Figure 50**. The maximum stress appeared at corner A in Hexagon Model 1 and the Circle Model, while it showed up at corner B in other models. Also, the Circle Model showed a considerably smaller maximum effective stress compared to the other models, suggesting that the Circle would be the best in terms of creating the minimum stress concentration in the matrix region,. If the adhesion condition between reinforcements and matrix was perfect in all models, the Circle Model would therefore show the highest strength.

Effect of Aspect Ratio on The Interface Stress Condition

The absolute values of maximum stresses at the interface under input stresses in the X- and Y-directions are shown in **Figure 51**. In the case where the input stress was applied in the Y direction, the maximum stress at the interface was increased with increasing aspect ratios. This result predicts that composites with higher aspect ratios would have lower strengths under such a condition. When input stress was applied in the X-direction, the maximum stress in the X-direction decreased with increasing aspect ratio while that in the Y-direction increased. These values reversed at the point where the aspect ratio was around 25. The shear stress on the interface showed the lowest value when the aspect ratio was around 50. There is thus probably an optimal aspect ratio to minimize stress concentration under this condition. If the fillers are randomly oriented in a composite, the tensile stresses will be the dominant factor since there should always be some fillers that are aligned parallel to the input stress.

The maximum effective stress values in the matrix region are summarized in **Figure 52**. The results showed the same tendency that the maximum stress at the interface did. Where input stress was applied in the Y-direction, the effective stress increased at large aspect ratios, with a minimum, however when the aspect ratio was around 20, suggesting there was an optimal aspect ratio to minimize stress concentration.

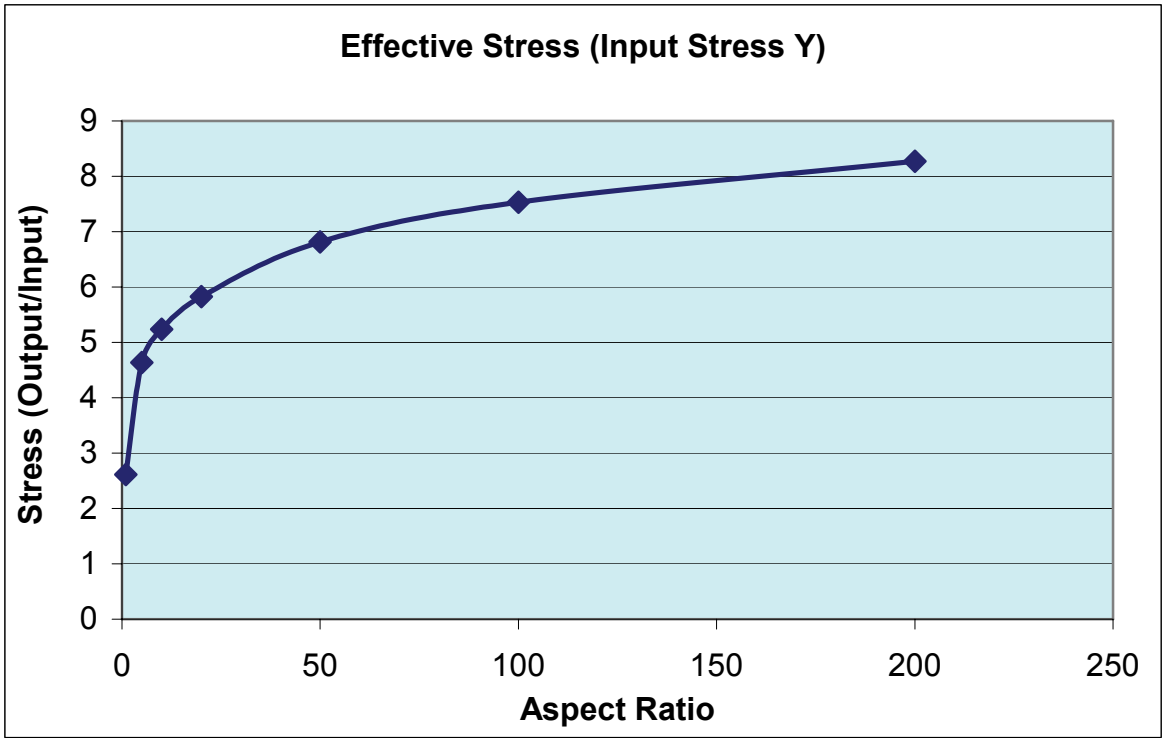

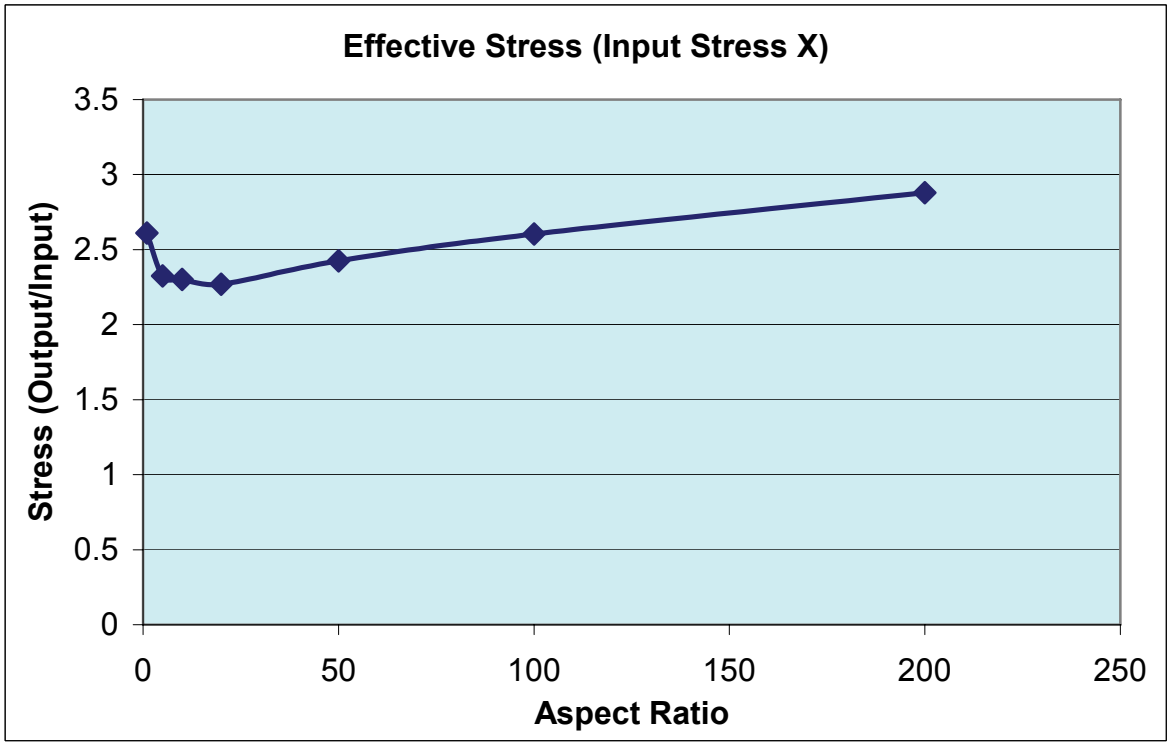

Figure 52. The effect of aspect ratio on the maximum effective stresses in matrix

Effect of Distance between Aligned Fillers

The maximum stresses at the interface are shown in **Figure 53**. All stresses increased with decreasing distance between the filler particles. Especially in the case of input stress in the Y-direction, the maximum stresses at the interface increased significantly when the distance became smaller. In the case of the input stress was applied in the X-direction, the maximum stresses showed the same tendency, but the output stress values were not as high as the former case. These results suggest that composites would fail at a lower input stress when the fillers are aligned and closely packed.

The maximum effective stress values in the matrix region are summarized in **Figure 54**. The results showed the same tendency that maximum stresses at the interface did. When the input stress was applied in the Y-direction, the effective stress increased significantly with decreasing distance. When the input stress was applied in the X-direction, the effective stress values were not as high as in the former condition. These results show that even if a composite system had perfect bonding between fillers and matrix, the matrix region would reach a yielding point at a lower input stress when the fillers were aligned and closely packed, leading to overall lower strength. Thus, this type of geometric arrangement is not good in terms of composite mechanical properties.

Effect of Distance between Parallel Fillers

The maximum stresses at the interface are shown in **Figure 55**. Compared to the other parameters, the spacing produced little change. Each stress did show a minimum value at some point, suggesting there was an optimal distance. Although the optimal point was somewhat different for each stress, it appeared near 5. The stress can transfer to neighboring fillers when they are located parallel, but the stress concentration effect overcomes this effect beyond some point.

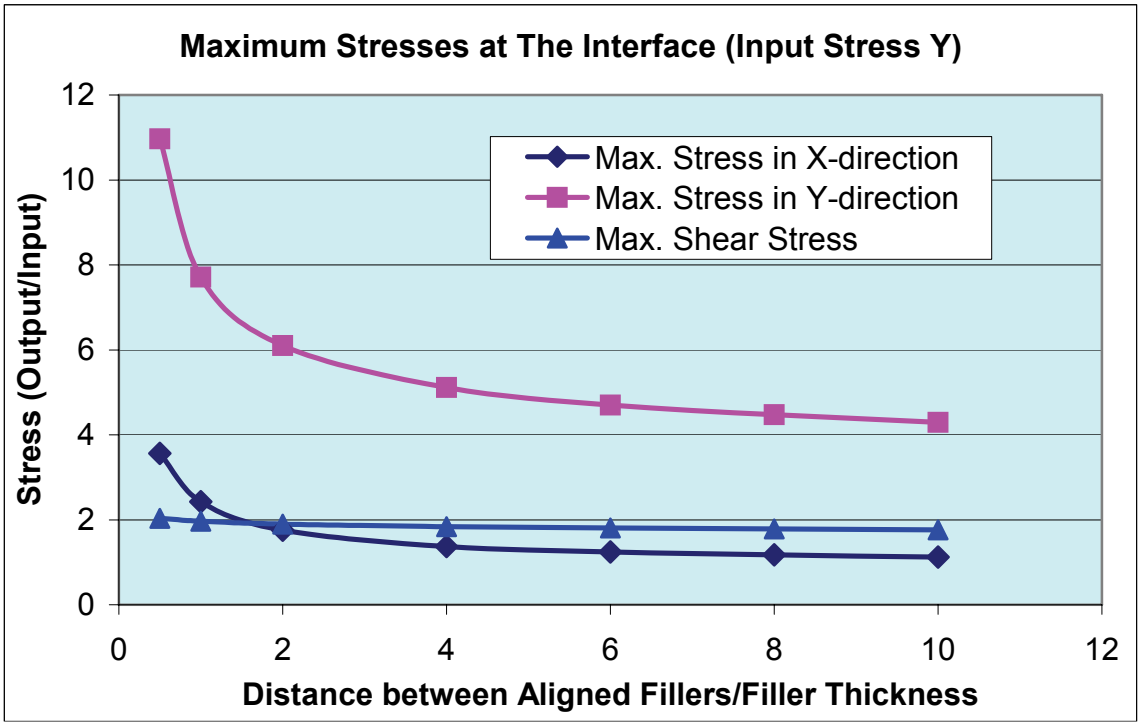

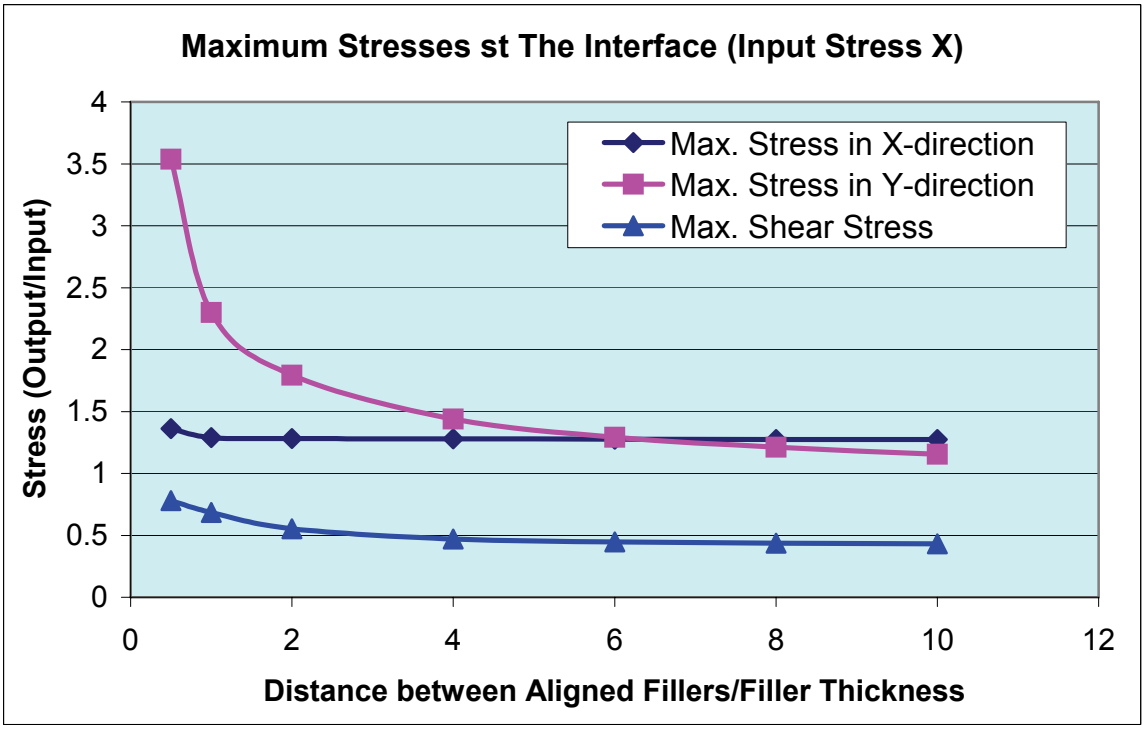

Figure 53. The effect of distance between aligned fillers on the absolute values of maximum stresses at the interface

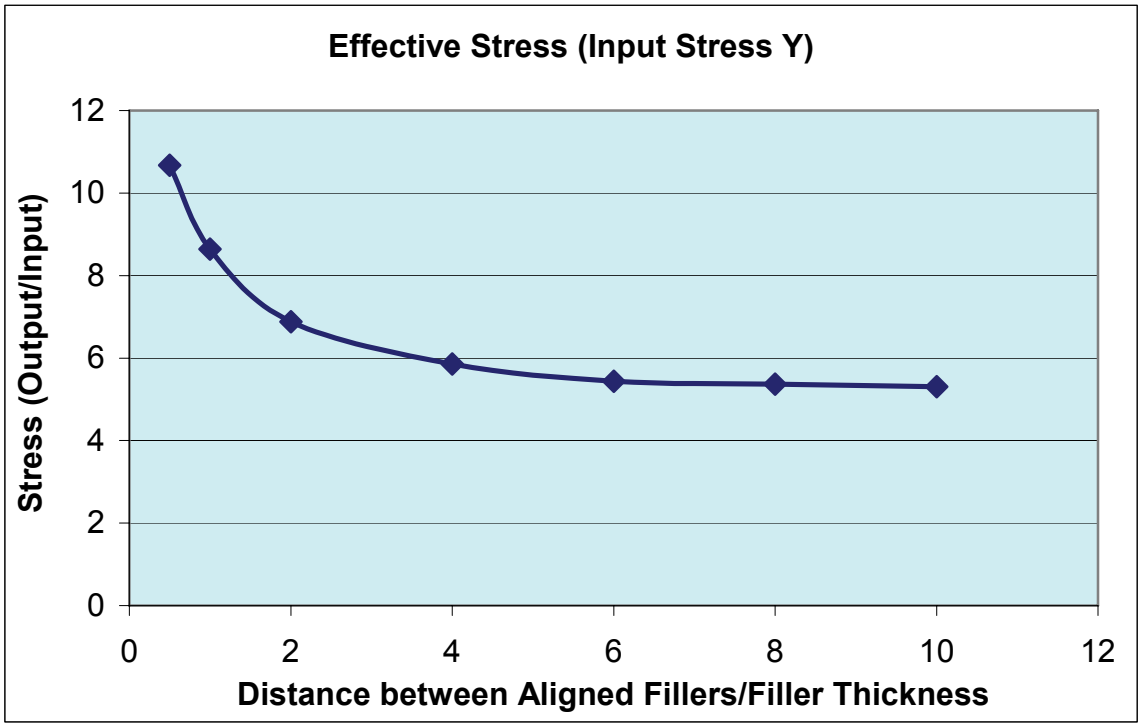

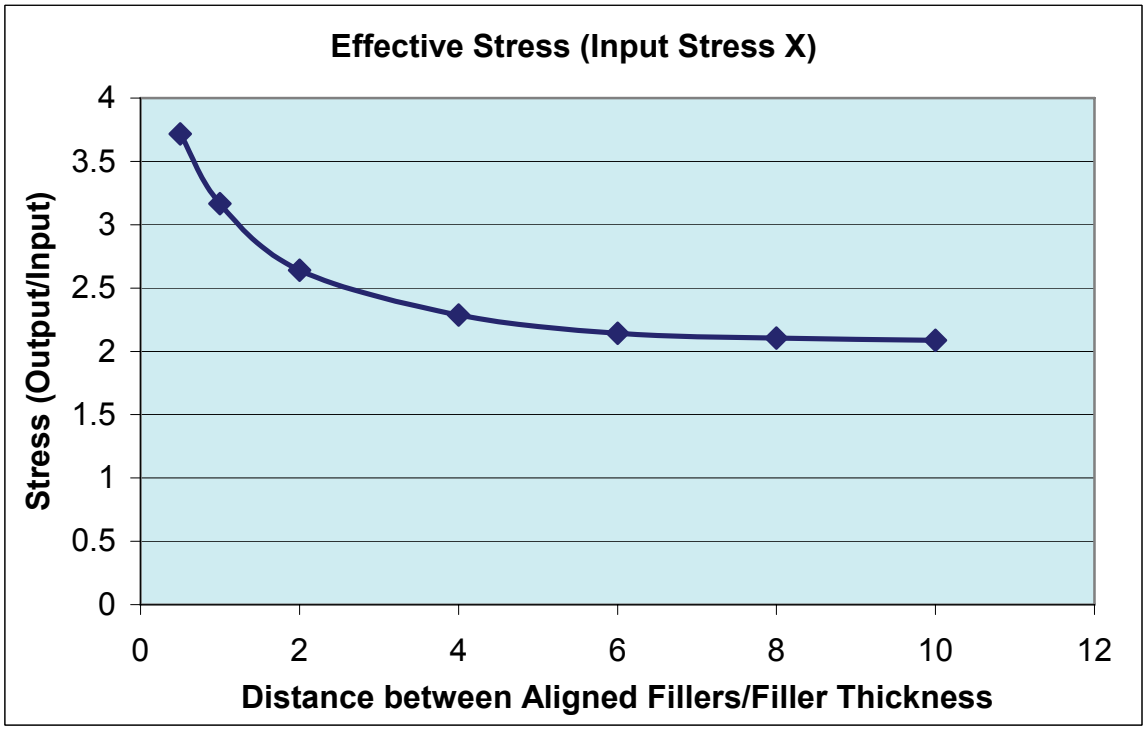

Figure 54. The effect of distance between aligned fillers on the maximum effective stresses in matrix

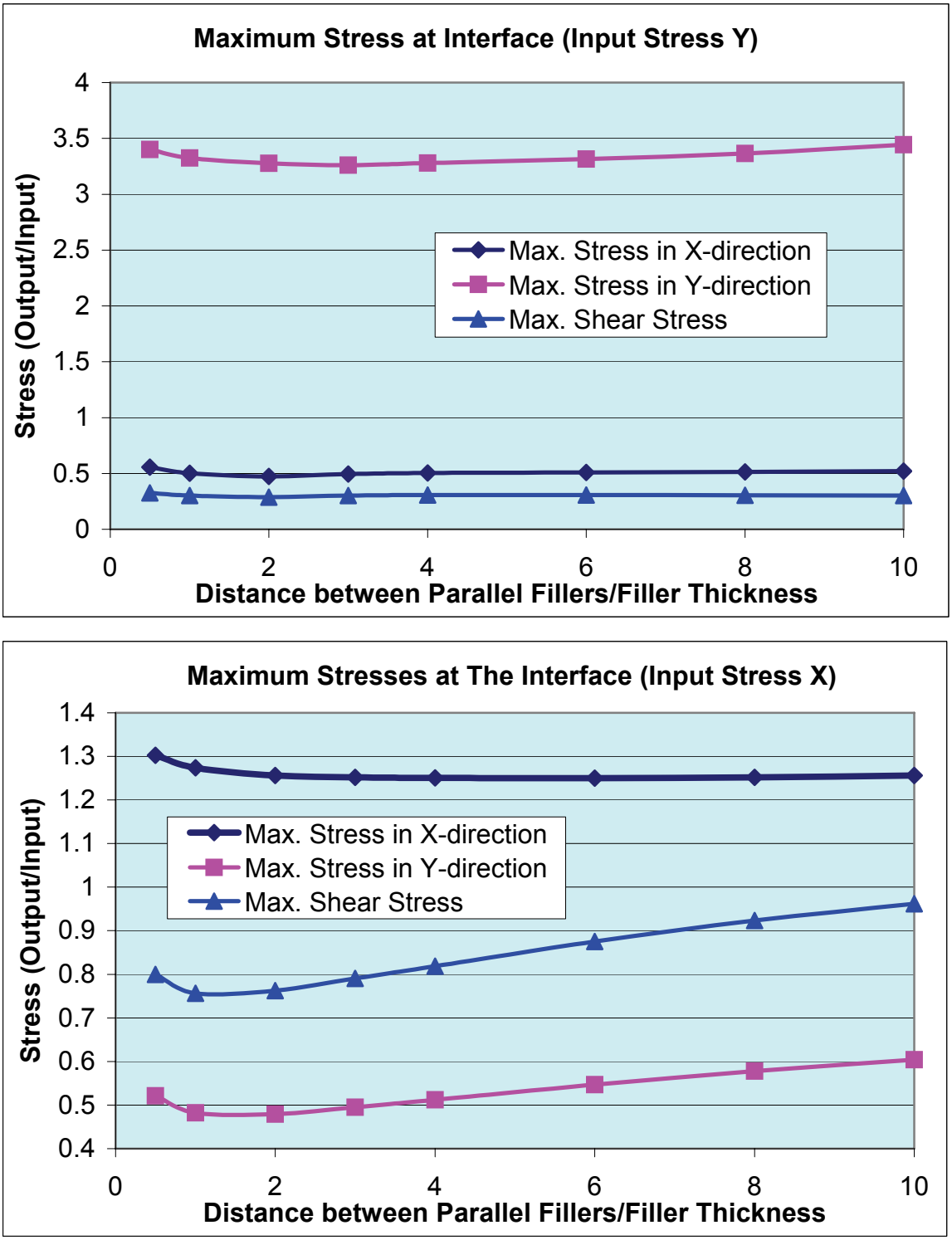

Figure 55. The effect of distance between parallel fillers on the absolute values of maximum stresses at the interface

The maximum effective stress values in the matrix region are summarized in **Figure 56**. These data show both X and Y stresses show a minimum at a distance around 6 to 8. Thus, the strength of a composite can be improved if the geometrical arrangement of fillers is controlled such that the system shows the optimal stress transfer condition.

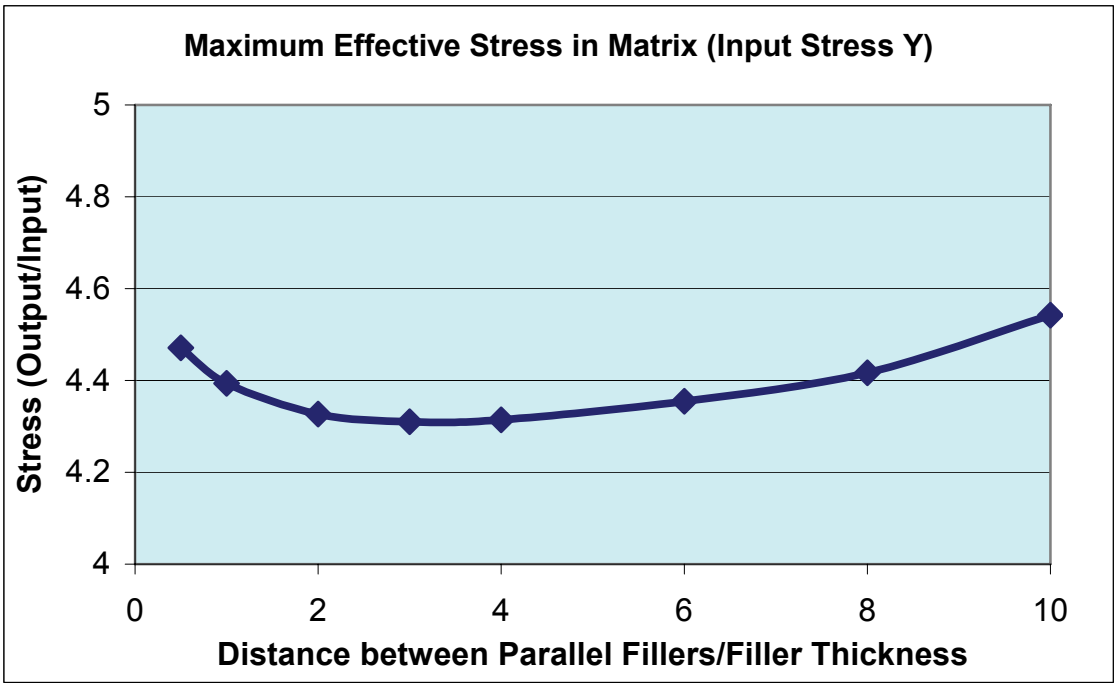

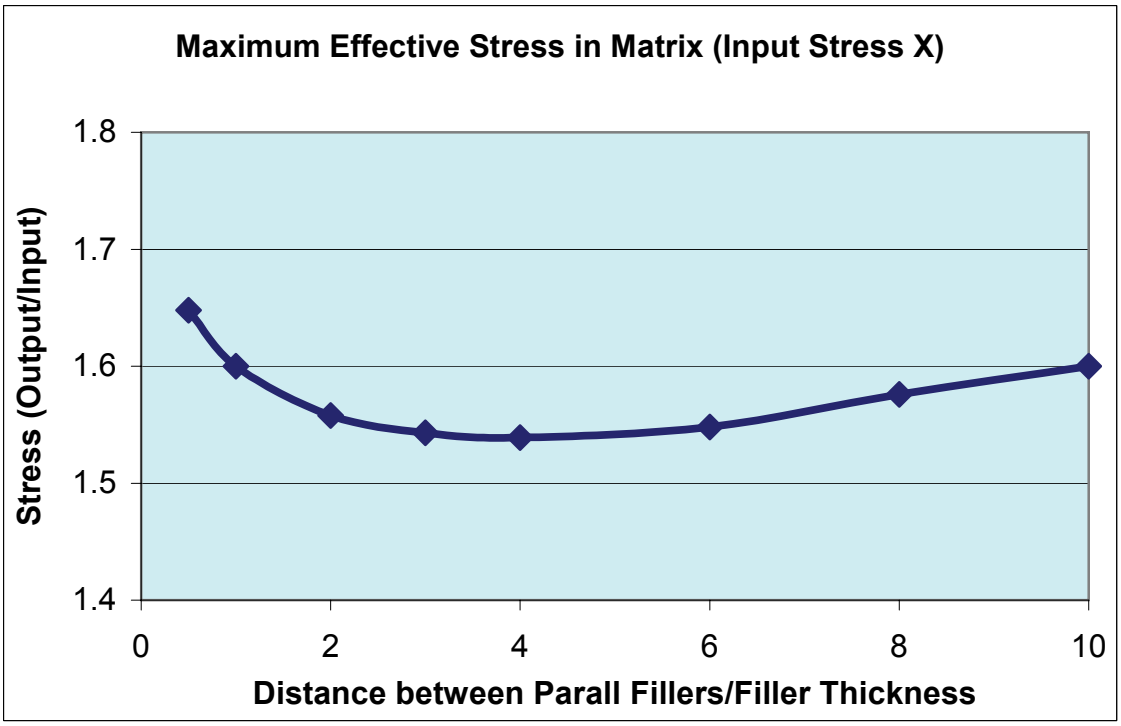

Figure 56. The effect of distance between parallel fillers on the maximum effective stresses in matrix

SUMMARY

Stress concentrations in composite systems were investigated by the finite element method and have led to the following conclusions:

• Corners with sharp angles introduce higher stress concentrations. Circular or round shapes produced the lowest stress concentration. Therefore, fillers with circular, ellipsoidal, or other rounded shapes should be better reinforcements in terms of minimizing the stress concentration.

• Fillers with higher aspect ratios introduced higher stress concentrations. This is especially important in nanocomposite systems, since nanoreinforcements often have very high aspect ratios.

• High stress concentration was introduced when fillers were aligned and located close to each other. This stress concentration could be very high when fillers were located close to each other at high volume fraction, whereas the stress concentration effect remained constant when fillers were separated by enough distance.

• The stress concentration was least when fillers were located parallel to each other at an optimal distance since stress could transfer from one filler to another.

If fillers are randomly oriented, they need to be separated sufficiently from each other to avoid creating high stress concentrations. In this case, the material may not reach the percolation concentration. To make the material conductive without sacrificing strength, it is necessary to arrange fillers close together, but in parallel positions so that they do not introduce a high stress concentration. The simulations revealed that there was an optimal distance for parallel-filler systems, which appeared to be around 2 to 4 times the thickness of the fillers. Thus, to maintain a distance between fillers such that tunneling occurs (about 10 nm at room temperature), the thickness of the fillers should be 5 nm or less. From these results, a nanocomposite morphology which could show good mechanical and electrical properties at the same time is proposed in **Figure 57**.

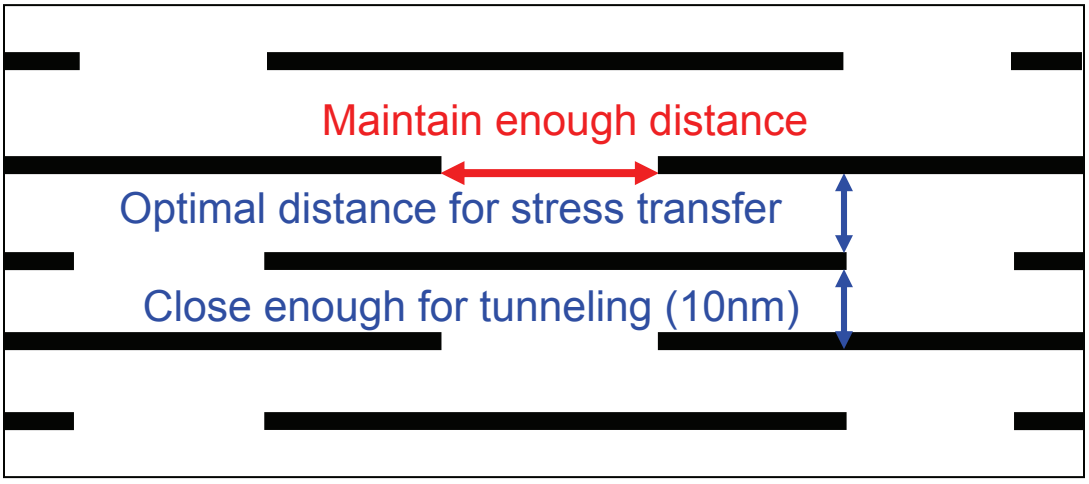

Figure 57. The optimal morphology for nanocomposite systems

REFERENCES

1. Whitesides, G. M., J. P. Mathisas, and C. T. Ceto, Science, **254**, 1312 (1991).
2. Gleiter, H. ,Adv. Mater., **4**, 474 (1992).
3. Novak, B. M., Adv. Mater., **5**, 422 (1993).
4. Komareni, S., J. Mater. Chem., **2**, 1219 (1992)
5. Philipp, G. and H. Schmidt, J. Non-cryst. Solids, **63**, 283 (1984)
6. Philipp, G. and H. Schmidt, J. Non-cryst. Solids, **82**, 31 (1986).
7. Huang, H. H., B. Orler, and G. L. Wilkes, Macromolecules, **20**, 1322 (1987)
8. Langley, R., G. C. Mbah, H. A. Freeman, H. H. Huang, E. J. Siochi, T. C. Ward, and G. Wilkes, J. Colloid Interface Sci., **143**, 309 (1991).
9. Ellsworth M. W., and B. M. Novak, Chem. Mater. **5**, 839 (1993)
10. Helbert, W., J. Y. Cavaille, and A. Dufresne, Polym. Compos., **17**, 604 (1996)
11. Hajji, J. Y. Cavaille, V. Favier, C. Gauthier, and G. Vigier, Polym. Compos., **17**, 612 (1996)
12. Favier, V., G. R. Canova, S. C. Shrivastava, and J. Y. Cavaille, Polym. Eng. Sci., **37**, 1732 (1997)
13. Giannelis, E. P., JOM, **44**, 28 (1992)
14. Giannelis, E. P. , Adv. Mater., **8**, 29 (1996)
15. Lan, T., and T. J. Pinnavaia, Chem. Mater., **6**, 2216 (1994)
16. Messersmith P. B. and E. P. Giannelis, Chem. Mater, **6**, 1719 (1994)
17. Gilman, J. W., T. Kashiwagi, and J. D. Lichtenhan, SAMPE Journal, **33**, 40 (1997)
18. Pinnavaia, T. J., T. Lan, P. D. Kavaritna, and M. S. Wang, Mater. Res. Soc., Symp. Proc.,346, Bett. Ceram. Chem., **6**, 81 (1994)
19. Messersmith P. B.\ and E. P. Giannelis, J. Polym. Sci. A: Polym. Chem., **33**, 1047 (1995)
20. Theng, B. K. G., 'The Chemistry of Clay-Organic Reactions', John Wiley and Sons, new York (1974)
21. Theng, 'B. K. G., 'Formation and Properties of Clay-Polymer Complexes', Elsevier Scientific Publication, New York (1979)
22. Proctor, A., and Sherwood, P. M. A., J. Electron Spectrosc. Relate. Phenom, 27, 39 (1982).
23. Xie, Y., and Sherwood, P. M. A., J. Appl. Spectros., 43, 7, 1153(1989).
24. Sherwood, P. M. A., "In Practical Surface Analysis by Ayger an X-Ray Photoelectron Spectroscopy, 2nd Edition.", Briggs and M. P. Seah editors, Wiley & Sons., (1990).
25. Xie, Y., and Sherwood, P. M. A., Chem. Mater., 1., 427, (1989).
26. Pittman, Jr., C. U., He, G-R., Wu, B., and Gardner, S. D., Carbon, 35, 3, 317 (1997).
27. Pittman, Jr., C. U., Wu, Z., Jiang, W., He, G-R., Wu, B., Li, W., and Gardner, S. D., Carbon, 35, 7, 929 (1997).
28. Yamada, K, Haraguchi, T., and Kajiyama, T., J. Appl. Polym. Sci., 75, 284 (2000). Son, Y., Noh, T. W., Lee, S. I., and Gaines, J. R., "Experimental Study of The Three-dimensional AC Conductivity and Dielectric Constant of a Conductor-Insulator Composite near the Percolation Threshold.", Phy. Rev. B 33, 2, (1986).
29. Lee, S. I., Song, Y., Noh, T. W., Chen, X. D., and Gaines, J. R., "Experimental Observations of Nonuniversal Behavior of The Conductivity Exponent for Three-dimensional continuum percolation systems.", Phys. Rev. B 34, 10, 6719 (1986).
30. Sato, N, Kurauchi, T, Sato, S., and Kamigaito, O, "SEM Observations of The Initiation and Propagation of Cracks in a Short Fiber Reinforced Thermoplastic Composite under Stress", J. Mater. Sci. Lett., 2, 188 (1983).
31. Eshelby, J. D., Proc. Roy. Soc. London, A241, 376 (1957).
32. Sato, N., Kurauchi, T, Sato, S., and Kamigaito, O., "Reinforcing Mechanism by Small Diameter Fiber in Short Fiber Composite." J. Compos. Mater., 22, 850 (1988).
33. Nardin, M and Schultz, J., "Interactions and Properties of Composites: a) Fiber-Matrix Adhesion Measurements." in "The Interfacial Interactions in Polymeric Composites.", Kliwer Academic Publishers, p81-93 (1993).
34. Mendelson, A., "Plasticity: Theory and Application", Robert E. Krieger Publishing Company, Malabar, Florida (1983).
35. Eshelby, J. D., "The continuum Theory of Lattice Defects, Progress in Solid State Physics, 3" Academic Press, New York (1956).
36. Mori, T. and Tanaka, K., "Average Stress in Matrix and Average Elastic Energy of Materials with Misfitting Inclusions." ACTA METALLURGICA, 21, 571 (1973).

37. Benveniste Y., “A New Approach to The Application of Mori-Tanaka Theory in Composite-Materials.’ Mech. Mater., 7, 2, 305, (1987)
38. Benveniste Y. Dvorak, G. J., and Chen, T., “Stress-fields in Composites with Coated Inclusions.” Mech. Mater., 7, 4, 305 (1989).
39. Zhu, H. and Achenbach J. D., “Radial Matrix Cracking and Interphase Failure in Transversely Loaded Fiber Composites.” Mech. Mater., 11, 4, 347 (1991).
40. Bigelow C. A., “The Effects of Uneven Fiber Spacing on Thermal Residual-stresses in a Unidirectional SCS-6/Ti-15-3 Laminate.” J. Compos. Technol. Res., 14, 4, 211 (1992).
41. Li, D. S., and Wisnom, M. R., “Finite-Element Micromechanical Modeling of Unidirectional Fiber-reinforced Metal-Matrix Composites.” Compos. Sci. & Technol., 51, 4, 545 (1994).
42. Sorense, B. F., and Talreja, R., “Effects of Nonuniformity of Fiber Distribution on Thermally-induced Residual Stresses and Cracking in Ceramic-matrix Composites.” Mech. Mater., 16, 4, 351 (1993).
43. Bohm, H. J., Rammerstorfer, F. G., Fischer, F. D., and Siegmund, T., “Microscale Arrangement Effects on The Thermomechanical Behavior of Advanced 2-phase Materials.” J. Eng. Mater. & Technol., 116, 3, 268 (1994).
44. Kouris, D. and Tsuchida, E., “On The Elastic Interaction between 2 Fibers in a Continuous Fiber Composite under Thermal Loading.” Mech. Mater., 12, 2, 131 (1991).
45. Kouris D., “Stress-concentration due to The Interaction between 2 Imperfectly Bonded Fibers in a Continuous Fiber Composite.” J. Appl. Mech., 60, 1, 203 (1993).
46. Kouris D. and Marshall, D., “Damage Mechanisms in Ti3Al Matrix Composites.” J. Eng. Mater. & Technol., 116, 3, 319 (1994).
47. Ebbessen, T. W., “Carbon Nanotubes: Preparation and Properties.”, CRC Press, Boca Raton, Florida, pp.5 (1997).